

Probabilistic dynamics of small groups in crowd flows

Chiel van der Laan^{1,2}, Alessandro Corbetta^{1,2,*},

1 Department of Applied Physics and Science Education, Eindhoven University of Technology, Eindhoven, The Netherlands

2 Eindhoven Artificial Intelligence Systems Institute, Eindhoven, The Netherlands

* a.corbetta@tue.nl

Abstract

Pedestrians in crowds frequently move as part of small groups, which can constitute up to 70% of individuals in public spaces. Dyads (groups of two) are most frequent. Understanding quantitatively the dynamics of dyads walking in crowds is therefore an essential building block towards a fundamental comprehension of the crowd behavior as a whole, and mandatory for accurate crowd dynamics models. Unavoidably, due to the non-deterministic behavior of pedestrians, characterizations of the dynamics must be probabilistic.

In this work, we analyze the dynamics of over $6 M$ dyads: a statistical ensemble of unprecedented resolution within a multi-year real-life pedestrian trajectory measurement campaign (about $21 M$ trajectories, collected in Eindhoven Central Station, The Netherlands). We provide phenomenological models for dyad behavior in dependence of the surrounding crowd's state. We present a thorough collection of fundamental diagrams that probabilistically relate both dyad velocity and dyad formation to the state of the surrounding crowd (density, relative velocity). Depending on the surrounding crowd, dyads adjust their interpersonal distance and may shift in formation, possibly turning from abreast states (known to favor social interaction) to in-line (which favors navigation through dense crowds). To quantitatively investigate formation changes, we introduce a scalar indicator, which we dub Orientation Log-Odds (OLO), that quantifies the relative log-likelihood of abreast versus in-file formations. Conceptually, for any given crowd state, the OLO quantifies energy difference of the abreast vs. in-file configuration under a Boltzmann-like assumption. We model how OLO depends on the crowd state, showcasing that its derivative is a product of two velocity-density fundamental diagrams.

Together, these results provide a statistically robust, data-driven description of dyad configuration dynamics in real-world crowds, establishing a foundation towards new predictive, group-aware crowd models.

Introduction

Understanding and quantitatively modeling pedestrian dynamics in crowds is essential for designing safe and comfortable civil infrastructures [1, 2], and is an outstanding scientific challenge, deeply connected with the statistical physics of active matter [3]. Prevalent in crowds are groups of individuals, i.e., *sets of people intentionally walking together* [4], which can account for even 70% of the whole mass [5] and do influence the collective dynamics [5–8]. Among groups, dyads, i.e., *two-person groups*, are the most frequent [5], with larger groups often fragmenting into stable two- or three-person subunits during movement [9]. Ultimately, this makes dyads one of the fundamental building blocks of collective pedestrian behavior. The characterization of group dynamics – and of dyads specifically – is therefore among the necessary ingredients towards predictive models for the crowd, and a must to surpass current modeling approaches where crowds are often only collections of independent agents [10]. Notably, due to stochasticity in pedestrian behavior, physical characterizations of groups have to be probabilistic, encompassing average trends, typical fluctuations, as well as unlikely states. Such a probabilistic characterization has been recently unlocked by advances in automated computer vision (e.g., [11–14]), which allowed the collection of anonymous, vast, real-life pedestrian trajectory datasets. Large trajectory datasets, even in the millions, have already unlocked detailed probabilistic characterizations of some pedestrian dynamics (e.g. in low density cases [15, 16], or effective/macroscopic descriptions at large spatial scales [12–14, 17–20]). The aim of this paper is to provide a thorough probabilistic characterization and phenomenological model of the behavior of dyads as macroscopic parameters of the surrounding crowd change.

A necessary aspect in the analysis of dyads and groups is their correct identification within the crowd. So far, group behavior has been extensively studied in controlled laboratory settings – where groups are defined *a priori* [7, 8, 21–25] – and through moderate-scale, real-life datasets, with groups identified through exhaustive human annotation. However, identification of groups manually, while obviously highly accurate, is very labor-intensive to scale beyond $\mathcal{O}(10^3)$ cases [5, 26–28]. Laboratory experiments, for example, in uni- and multidirectional flows and bottleneck scenarios (cf. review in [10] for an overview) have provided first approximations to macroscopic descriptors, such as relation between densities and group velocities (so-called fundamental diagrams [7, 8, 21, 22]). Yet, limited participant numbers, typically fewer than one hundred units, have bottle-necked finer-scale investigation, e.g., of fluctuation around ensemble averages. Conversely, research based on real-life datasets has enabled more detailed microscopic analyses, e.g., in the case of a dyad walking in complex environments [5, 29]. It has been observed how the crowd surrounding a dyad has impact, for instance, in its spatial formation: a dyad can transition from abreast configuration (pedestrians side-by-side, efficient for communication [30]) possible low density, to in-file, that streamlines motion in higher density regimes [29].

A quantitative probabilistic characterization of how dyads behave as we change critical parameters such as their walking speed and the density and relative speed of the surrounding crowd, ultimately yielding also changes of formation, has remained, however, beyond the statistical resolution of current investigations. Inevitably, to analyze group dynamics in datasets

surpassing $\mathcal{O}(\gg 10^3)$ trajectories, routine in recent data collections, the group identification has to be automated. Anonymity in data collection, often mandatory when operating in public spaces, limits measurements to trajectories only, and generates a substantial technical challenge. In other terms, pedestrians are reduced to positional information only, with no additional kinematic or anatomical feature – this forbids tracking and group detection hinging on visual cues (e.g. appearance and body language [31–33]). With the exclusive availability of trajectories of centers of mass, group detection can only rely on proxemics indicators, with heuristics aimed at distinguishing genuine groups from coincidental proximity [34–38]. Heuristics proposed consider the time-consistency or spatio-temporal clustering of distances [34–36], sufficient correlation [39] in velocities or even gait [38]. A key bottleneck is the computational cost of pair-wise metrics/correlation indicators among all trajectories pairs in space and time. To this purpose, in [36] some authors of this work proposed a graph-based additive algorithm requiring a single pass in time of the dataset, allowing the extraction of groups within datasets of size $\mathcal{O}(10^4)$.

In this study, we investigate and characterize probabilistically how a crowd surrounding a dyad determines its kinematics, e.g. in terms of dyad velocity, relative distance of the dyad components and, in general, the spatial formation. We show how the crowd has different effects in dependence on its density as well as on the relative flow with respect to the dyad, considering counter-flowing, standing, and co-flowing crowds. Respectively, these are cases in which the crowd velocity is opposed, vanishes, and has the same orientation with respect to the dyad velocity. To this purpose, we establish an unprecedented dataset composed of $\mathcal{O}(10^6)$ dyads that have been part of the highly variable daily crowd traffic at a train platform in Eindhoven, The Netherlands (cf. Fig 1a). Specifically, we derive a comprehensive set of fundamental diagram-like relationships, revealing how dyad configuration is modulated by the surrounding crowd. To move beyond descriptive statistics and enable predictive modeling, we introduce a scalar indicator, that we dub *Orientation Log-Odds* (OLO), quantifying the relative probability of a dyad to be in abreast vs. in-file configuration. Not only through the OLO indicator we provide a probabilistic characterization of how formation is influenced by crowd variables and dyad velocity, but also we show how such indicator can be phenomenologically modeled, with high accuracy, as a product of fundamental diagram-like relations connected with local minima and maxima of the formation probability. We constructed our dyad dataset by automatically identifying 6 M dyads throughout the exhaustive tracking data collected at Eindhoven train station between March 2021 and March 2024 (avg. 24 k trajectories per day; [40, 41]). To achieve scalable dyad identification, we build on the graph-based method in [36] and efficiently classify groups based on joint time-consistency of distance. Overall, our computational and modeling framework allows us, for the first time, to provide accurate phenomenological models for the dyad behavior (velocity and configuration) across the full spectrum of crowd densities and flow regimes observed: free flows, co-, counter-flows, and flows through standing crowds.

The reminder paper is structured as follows: in Section 1, we describe our dataset and analysis pipeline. We introduce the large-scale pedestrian trajectory dataset from Eindhoven Central Station, define the coordinate

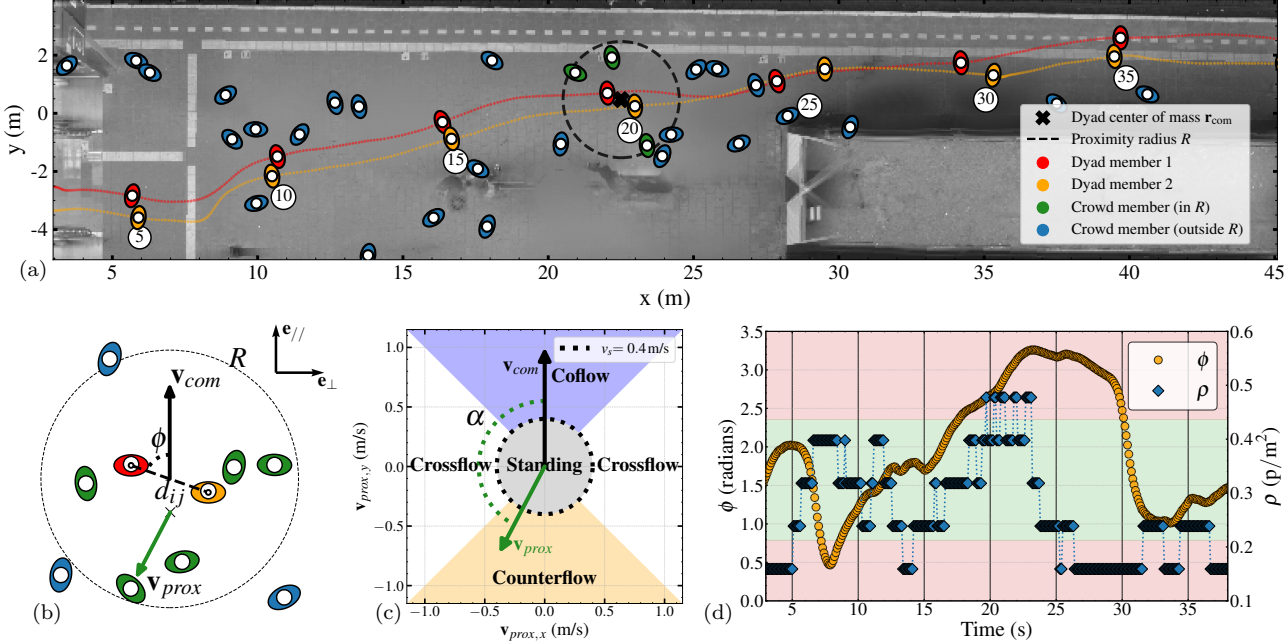


Fig 1. Example dyad trajectory and definition of dyad observables. (a) Section of Eindhoven Central Station platform 3-4 with an example trajectory (red and orange lines) of a dyad entering from the bottom left and moving toward the top right of this domain. The red and orange markers show the dyad member positions at 5 s intervals. Other pedestrians positions (blue) are from a snapshot at time 20 s; at this time the dashed circle marks a 2 m proximity radius around the dyad center of mass \mathbf{r}_{com} with pedestrians inside colored in green. (b) Observables in the dyad's frame of reference. The dyads frame of reference is defined by the basis $(\mathbf{e}_{\parallel}, \mathbf{e}_{\perp})$ (Eq 4), where the centre-of-mass velocity \mathbf{v}_{com} (Eq 3) is parallel to v_{\parallel} . Besides \mathbf{v}_{com} , the interpersonal distance d_{ij} , and the dyad angle $\phi = -\text{atan2}(x_r, y_r)$ are illustrated, where atan2 is the two-argument arctangent function. Considered observables that depend on crowd members within the radius R are their mean velocity \mathbf{v}_{prox} and local density ρ (Eq 11, here $\rho = 0.56 \text{ p/m}^2$). (c) Dyad-crowd interaction regimes B (Eq 14) defined in dependence on \mathbf{v}_{prox} and the angle α . We shall consider dynamics on only in free-flow (no crowd), co-, counter-flow and with standing crowd. (d) ϕ and ρ over time as the dyad in (a) traverses the domain, highlighting the abreast (red) and in-file (green) regions. The vertical lines correspond time snapshots in (a). Between $t = 15 \text{ s}$ and $t = 35 \text{ s}$ the dyad enters a region of higher ρ , temporally going in in-file formation before going back to an abreast formation.

system and key observables, and detail the unsupervised dyad detection methodology. In Section 2, we present a comprehensive empirical characterization of dyad dynamics. This includes an analysis of fundamental-diagram relationships across various regimes, and conditional analyses of distance and positions. We also introduce our *Orientation Log-Odds* (OLO), scalar indicator for the probability of the dyad configuration (abreast vs. in-file). In Section 3, we characterize and model OLO behavior across crowd conditions of increasing complexity, from free-flow conditions, progressing to static crowds, and finally a general scenario including co- and counter-flows. The discussion in Section 4 closes the work.

1 Dataset, statistical observables, and unsupervised dyad identification

This study considers the dynamics of dyads walking at Eindhoven Central Station on platform 3-4. Eindhoven Central Station is the fifth-largest station in the country. We leverage on an anonymous trajectory dataset of 900 days collected over a three-year period from March 2021 to March 2024 [40], (cf. other usages e.g. in [18, 41, 42]). The measurement setup performed 24/7 anonymous crowd tracking over a $80\text{ m} \times 10\text{ m}$ area, with 10 Hz time resolution, via a grid of overhead sensors (cf. Fig 1, see [41, 42] for the methodology). The dataset includes about 24 k pedestrian trajectories per weekday across various density levels, typically ranging from 0 to 1.3 p/m^2 , with occasional outliers reaching up to 2 p/m^2 . To filter out measurement noise, each trajectory is smoothed using a Savitzky-Golay filter, and the first and last two seconds are excluded to avoid artifacts from partially observed motion at the edges of the sensing area.

To identify, parametrize and analyze the state of dyads, we focus on four key observables which proxy the local dynamics of the dyad and the hydrodynamic/macrosopic state of the surrounding crowd. Note that the anonymous nature of the data (trajectory only) constrains our parameter choice to kinematic observables, making our choice possibly the simplest. Postponing formal definitions to the next Section 1.1, for each dyad, at each time instant, we consider the vector state

$$(\mathbf{r}_{loc}, \mathbf{v}_{com}, \rho, \mathbf{v}_{prox}), \quad (1)$$

where

- \mathbf{r}_{loc} [m] – relative position of the dyad members in the coordinate system of the center of mass;
- \mathbf{v}_{com} [m/s] – dyad velocity, in terms of its center of mass;
- ρ [p/m²] – local density of the crowd surrounding the dyad;
- \mathbf{v}_{prox} [m/s] – (hydrodynamic) velocity of the crowd surrounding the dyad.

We will work with convenient derived quantities, these range from the distance between dyad members, to the ownership to a specific flow regime that are too computed as functions of Eq 1. Specifically, our characterization will be probabilistic, and we will work with suitable conditioned (marginal) probability or conditional statistics of the law

$$\mathbb{P}(\mathbf{r}_{loc}, \mathbf{v}_{com}, \rho, \mathbf{v}_{prox}), \quad (2)$$

which we empirically estimate through our dataset. Moreover, we will use the symbol $\boldsymbol{\theta}$ to denote either generic some conditioning variables (either generic or defined within the section).

The observables in Eq 1 are also instrumental for the unsupervised identification of dyads in anonymous data, that is the object of the Section 1.2.

1.1 Observables and coordinate system

Kinematic state of a dyad. Given a dyad of two pedestrians, so forth indexed with 1 and 2, with instantaneous positions $(\mathbf{r}_1, \mathbf{r}_2)$ and velocities $(\mathbf{v}_1, \mathbf{v}_2) = (\dot{\mathbf{r}}_1, \dot{\mathbf{r}}_2)$, we adopt a co-moving coordinate system centered on the dyad's center of mass (see Fig 1b), in the same spirit of [30] by Zanlungo et al. The center of mass position \mathbf{r}_{com} and velocity \mathbf{v}_{com} are,

$$\mathbf{r}_{\text{com}} = \frac{\mathbf{r}_1 + \mathbf{r}_2}{2}, \quad \mathbf{v}_{\text{com}} = \dot{\mathbf{r}}_{\text{com}} \frac{\mathbf{v}_1 + \mathbf{v}_2}{2} = \|\mathbf{v}_{\text{com}}\| \mathbf{e}_{\parallel}, \quad (3)$$

where the last equality is expressed in terms of the local basis

$$\mathbf{e}_{\parallel} = \frac{\mathbf{v}_{\text{com}}}{\|\mathbf{v}_{\text{com}}\|}, \quad \mathbf{e}_{\perp} = R_{90^\circ} \mathbf{e}_{\parallel}, \quad (4)$$

in which \mathbf{e}_{\parallel} is parallel to \mathbf{v}_{com} and \mathbf{e}_{\perp} is perpendicular (with $\|\cdot\|$ being the Euclidean norm). This basis is ill-defined in case a dyad is standing, since small instantaneous fluctuations (due to body oscillation or measurement noise) map into erratic \mathbf{e}_{\parallel} directions. Since we are interested in walking dyads, we set a “standing” velocity threshold at set the standing threshold at $v_s = 0.4 \text{ m/s}$, and require that the walking speed

$$\mathbf{v}_{\text{com}} = \|\mathbf{v}_{\text{com}}\| \quad (5)$$

satisfies

$$\mathbf{v}_{\text{com}} > v_s. \quad (6)$$

Note that we choose v_s between the standing ($\mathbf{v}_{\text{com}} = 0$) and slow-walking ($\mathbf{v}_{\text{com}} \approx 0.6 \text{ m/s}$) peaks in the velocity distribution (see Appendix A, Fig 11). v_s remains well below the normal walking speed ($\approx 1.3 \text{ m/s}$). In this basis, which is depicted in Fig 1b, the relative positions of the dyad members can be rewritten as

$$\mathbf{r}_{\text{loc}1} = x_r \mathbf{e}_{\parallel} + y_r \mathbf{e}_{\perp}, \quad \mathbf{r}_{\text{loc}2} = -\mathbf{r}_{\text{loc}1} = -x_r \mathbf{e}_{\parallel} - y_r \mathbf{e}_{\perp}, \quad (7)$$

where (x_r, y_r) are the components of the relative position transverse and longitudinal to \mathbf{e}_{\parallel} . In this reference, the distance, d , between the dyad members can be conveniently written as

$$d = 2\|\mathbf{r}_{\text{loc}1}\| = 2\sqrt{x_r^2 + y_r^2}. \quad (8)$$

The (x_r, y_r) coordinates allows us to establish a quantitative definition for abreast and in-file dyad formation, which we regulate through an even partition of the (x_r, y_r) plane into two cones of identical volume, Γ^{\leftrightarrow} and Γ^{\uparrow} , bordered by the 45° bisectors. In formulas, we define

$$\text{Abreast} \Leftrightarrow (x_r, y_r) \in \Gamma^{\leftrightarrow} = \{(x_r, y_r) \mid x_r^2 - y_r^2 \geq 0\}, \quad (9)$$

$$\text{In-file} \Leftrightarrow (x_r, y_r) \in \Gamma^{\uparrow} = \{(x_r, y_r) \mid x_r^2 - y_r^2 < 0\}. \quad (10)$$

In other terms, we name abreast any configuration in which the angle between the relative position and the velocity $\phi = \arctan(y_r/x_r)$ is larger than 45° and in-file otherwise. Note that the abreast and in-file regions of the (x_r, y_r) plane are identical but a $\pm 90^\circ$ degree rotation.

Hydrodynamic state of the crowd surrounding a dyad. To parametrize the state of the crowd surrounding a dyad, we consider local estimates of the density ρ and of the crowd velocity \mathbf{v}_{prox} within a radius of $R = 2$ m around the dyad center of mass \mathbf{r}_{com} .

Specifically, we define the local density as

$$\rho = \frac{N_R}{\pi R^2}, \quad (11)$$

where N_R denotes the total number of pedestrians within the proximity radius (including the dyad members). By extension, the density for a dyad in free flow (i.e., $N_{prox} = 2$) is $\rho_{free} = 0.16$ p/m². The corresponding proxy crowd velocity is given by the mean velocity of the pedestrians in this region,

$$\mathbf{v}_{prox} = \frac{1}{N_{prox}} \sum_{\substack{i=1 \\ i \notin \text{dyad}}}^{N_{prox}} \mathbf{v}_i, \quad (12)$$

where $N_{prox} = N_R - 2$ represents the number of pedestrians within the proximity radius, excluding the dyad members themselves.

The two velocities \mathbf{v}_{com} and \mathbf{v}_{prox} allows isolating different regimes of relative motion between the dyad and the crowd, including, but not limited to, flow through a standing crowd, co-flow, and counter-flow. To this purpose, let α be the oriented angle between these two velocities, i.e.

$$\alpha = \alpha(\mathbf{v}_{com}, \mathbf{v}_{prox}) = \text{atan2}(\|\mathbf{v}_{com} \times \mathbf{v}_{prox}\|, \mathbf{v}_{com} \cdot \mathbf{v}_{prox}), \quad -\pi \leq \alpha \leq \pi, \quad (13)$$

where $\text{atan2}(\cdot)$ is the two-argument arctangent function (positive for counterclockwise angles from \mathbf{v}_{com} and negative otherwise). We use the angle α together with the velocity magnitude $\|\mathbf{v}_{prox}\|$ to exhaustively classify the dyad-crowd dynamics into five non-overlapping regimes, also depicted in Fig 1c:

$$B(\alpha, \|\mathbf{v}_{prox}\|) = \begin{cases} B_{free} & \text{if } N_{prox} = 0 \\ B_{standing} & \text{if } \|\mathbf{v}_{prox}\| < v_s = 0.4 \text{ m/s} \\ B_{coflow} & \text{if } \|\mathbf{v}_{prox}\| \geq v_s \wedge |\alpha| < \pi/4 \\ B_{counterflow} & \text{if } \|\mathbf{v}_{prox}\| \geq v_s \wedge |\alpha| > 3\pi/4 \\ B_{crossflow} & \text{if } \|\mathbf{v}_{prox}\| \geq v_s \wedge \pi/4 \leq |\alpha| \leq 3\pi/4 \end{cases} \quad (14)$$

B_{free} identifies the free flow regime, in which the dyad is surrounded by no other pedestrian within radius R . We identify a crowd standing around the dyad by limiting $\|\mathbf{v}_{prox}\|$ by the previously defined threshold v_s . When $\|\mathbf{v}_{prox}\| > v_s$ we consider the crowd moving, which we further separate, based on α , in co-flowing, counter-flowing and cross-flowing regimes. Also in this case we use the cones along the 45° bisectors as boundaries.

In the following we opt to focus on free-flow, standing, co- and counter-flow regimes as prototypes of the interaction scenarios, and neglect the many corner cases of the cross-flow regimes in which a dyad traverses (or is traversed), by a crowd moving sideways with respect to its own velocity.

Within the considered discrete regimes B (Eq 14), in the cases B_{free} and $B_{standing}$ – Eq 1 reduces to two variables, $(\mathbf{r}_{loc}, \mathbf{v}_{com})$, and three variables, $(\mathbf{r}_{loc}, \mathbf{v}_{com}, \rho)$, respectively – whereas for $B_{counterflow}$ and

B_{coflow} Eq 1 retains the full four-parameter complexity. We introduce therefore a final dimensionless velocity ratio that quantifies the projection of the crowd velocity onto the dyad's direction of motion for non-standing crowds, which approximates both relative velocity of dyad and crowd and proxies the regimes, and which we will use to parametrize continuously between these flow states:

$$\tilde{v}_{\parallel} = \frac{\mathbf{v}_{\text{prox}} \cdot \mathbf{v}_{\text{com}}}{\|\mathbf{v}_{\text{com}}\|^2} = \frac{\|\mathbf{v}_{\text{prox}}\|}{\|\mathbf{v}_{\text{com}}\|} \cos \alpha \quad \text{for } \|\mathbf{v}_{\text{prox}}\| > v_s \quad (15)$$

This scalar quantity has two key properties:

1. the sign of \tilde{v}_{\parallel} discriminates among relative flow regime of dyad and crowd and provides a continuous yet approximate proxy of the regimes in Eq 14, specifically
 - when $\tilde{v}_{\parallel} > 0$ dyad and crowd move in the same direction (co-flow) and $\tilde{v}_{\parallel} \in (v_s, \infty)$ approximates B_{coflow} ;
 - when $\tilde{v}_{\parallel} < 0$ they move in opposite direction (counter-flow) and $\tilde{v}_{\parallel} \in (-\infty, -v_s)$ approximates $B_{\text{counterflow}}$.
2. The magnitude of \tilde{v}_{\parallel} scales as the speed ratio: when \mathbf{v}_{prox} and \mathbf{v}_{com} are parallel ($|\cos \alpha| = 1 \Rightarrow |\alpha| \in \{0, \pi\}$), \tilde{v}_{\parallel} directly represents the crowd-to-dyad speed ratio. For example, $|\tilde{v}_{\parallel}| = 1$ indicates matched speeds (dyad and crowd move at the same speed either in co- or counter-flow), $\tilde{v}_{\parallel} = 2$ means the crowd moves twice as fast as the dyad, and so on. Moreover, since $\|\mathbf{v}_{\text{prox}}\| > v_s$, $|\tilde{v}_{\parallel}|$ can only be small if $\|\mathbf{v}_{\text{com}}\|$ is large (i.e. the dyad is faster than the crowd). Finally, any incidence angle α such that $|\cos \alpha| < 1$ reduces the \tilde{v}_{\parallel} magnitude, but since we neglect $B_{\text{crossflow}}$, such a reduction satisfies $|\cos \alpha| > \sqrt{2}/2 \approx 0.71$.

1.2 Unsupervised detection of dyads

Here we describe the approach to automatically identify dyads within our dataset. As we work with anonymous trajectory data, the approach can rely only on trajectory properties and heuristically classify dyads relying on how mutual proximity is sustained over time. The technical challenge is distinguishing between genuine dyads and trajectories that came into contact by chance. We combine two approaches previously proposed [15, 36], and model pedestrians in a crowd as nodes in a graph. Edges carry information about guessed pairwise interactions or lack thereof. In this graph, group dyads will be connected components of size 2 after suitable pruning.

More formally, let us indicate with $\mathbf{r}_i(\cdot)$ the trajectory of pedestrian i , defined between their entry and exit times, say the interval $\mathcal{T}_i = [t_{i,0}, t_{i,f}]$. Our graph G has the set of all trajectories as base. We initialize the edge set \mathcal{E}_0 including all pedestrian pairs appearing together in our measurement area and thus potentially part of a group

$$\mathcal{E}_0 = \{(\gamma_i, \gamma_j), i > j \mid \mathcal{T}_i \cap \mathcal{T}_j \neq \emptyset\}. \quad (16)$$

Since we focus on walking dyads (rather than standing ones), we introduce the temporal domain in which both pedestrian are walking, i.e. where both

pedestrians move faster than the standing threshold v_s . This gives us the walking temporal domain $\tilde{\mathcal{T}}_{ij}$:

$$\tilde{\mathcal{T}}_{ij} = \{ t \in \mathcal{T}_i \cap \mathcal{T}_j \mid \|\mathbf{v}_i(t)\| > v_s, \|\mathbf{v}_j(t)\| > v_s \}, \quad (17)$$

For any trajectory pair $(\mathbf{r}_i(\cdot), \mathbf{r}_j(\cdot)) \in \mathcal{E}_0$ we compute their distance

$$d_{ij}(t) = \|\mathbf{r}_i(t) - \mathbf{r}_j(t)\|, \quad \forall t \in \mathcal{T}_i \cap \mathcal{T}_j, \quad (18)$$

of which we retain the time-average

$$\langle d_{ij} \rangle_t = \langle d_{ij}(\cdot) \rangle_t = \frac{1}{|\mathcal{T}_i \cap \mathcal{T}_j|} \int_{\mathcal{T}_i \cap \mathcal{T}_j} \|\mathbf{r}_i(t) - \mathbf{r}_j(t)\| dt. \quad (19)$$

To ensure prolonged proximity while walking we only consider pairs who are in the scene together for t_{max} and are walking for at least \tilde{t}_{max} . Generalizing the discrete approach in [36], we retain only edges having $\langle d_{ij} \rangle_t$ below a threshold d_{max} :

$$\mathcal{C} = \left\{ (\mathbf{r}_i(\cdot), \mathbf{r}_j(\cdot)) \in \tilde{\mathcal{E}} \mid \begin{array}{l} |\mathcal{T}_i \cap \mathcal{T}_j| > t_{max} \\ |\tilde{\mathcal{T}}_{ij}| > \tilde{t}_{max} \\ \langle d_{ij} \rangle_t < d_{max} \end{array} \right\} \subset \tilde{\mathcal{E}}, \quad \begin{array}{ll} t_{max} = 8.0 \text{ s} \\ \tilde{t}_{max} = 4.0 \text{ s} \\ d_{max} = 1.5 \text{ m} \end{array} \quad (20)$$

Thus, \mathcal{C} defines the edges of a graph connecting pedestrians in the same group, where connected component size indicates group size.

Finally, to isolate dyads, we use the approach from [15] and retain only those graph elements whose connected components size is exactly two.

Note that the *average* distance threshold employed, d_{max} , turns out to be a very generous over-estimate of the typical, and often even maximum distance of the dyads considered (as will be outlined in the forthcoming sections). As such, considering also the scale of the dataset, our result have practically no sensitivity to perturbation of d_{max} of even 30% – 40%. It is worth mentioning that also requiring dyads to have velocity correlation above a threshold (conjecturing that a pair walking together should have velocity fluctuations in phase/counter-phase) makes no practical difference at our scale (while possibly be detrimental in case of smaller sets: dyad could have velocity fluctuations in counter-phase, or decorrelated at slow center of mass velocity).

2 Large-scale empirical analysis of dyad configuration dynamics and crowd-dependent formation changes

We consider here how dyad depend probabilistically on the various crowd conditions, on the basis of our multi-year dataset (Section 1). Our analysis centers on conditional dependencies within the four-dimensional state vector $(\mathbf{r}_{loc}, \mathbf{v}_{com}, \rho, \mathbf{v}_{prox})$ introduced in Eq 1, which includes variations on the typical fundamental diagrams and beyond, with increasing microscopic detail:

(i) *Fundamental diagrams* ($\mathbb{E}[\mathbf{v}_{com} | \rho, \mathbf{r}_{loc}, B]$) which include speed-density relationships to provide baseline characterization of dyad behavior and comparison with non-dyad pedestrians across different configurations and interaction regimes.

- (ii) *Configuration heatmaps* ($\mathbb{P}(x_r, y_r \mid v_{\text{com}}, \rho, B)$), which analyze how the full spatial distribution of dyad configurations changes as functions of speed, density, and flow regime to reveal systematic transitions between preferred states.
- (iii) *Relative-position diagrams* ($\mathbb{E}[\rho | \mathbf{r}_{\text{loc}}]$ and $\mathbb{E}[v_{\text{com}} | \mathbf{r}_{\text{loc}}]$), examining how environmental conditions vary spatially within the dyad local coordinate frame to identify the typical crowd states associated with different relative positions.
- (iv) *Interpersonal distance analysis* ($\mathbb{E}[d | \rho]$), quantifying how (modal) distances between dyad members depend on density and configuration. These analyses reveal systematic shifts between abreast and in-file configurations due to both density and surrounding flow conditions.

Finally, in Section 2.2 we reduce the relative likelihood of each configuration in parameter space to a scalar measure – which we dub Orientation Log-Odds (OLO) – that captures the preference between abreast versus in-file configurations, enabling quantitative modeling of dyad formation dynamics.

2.1 Analysis of configuration-dependent dyad behavior in varying environment

Fundamental diagrams. To establish a baseline characterization of dyad configurations, we analyze speed-density relationships (i.e. fundamental diagrams, $\mathbb{E}[v_{\text{com}} | \rho]$) and compare dyad and non-dyad pedestrian speeds across different interaction regimes. In Fig 6a, we show the relationship between dyad speed, v_{com} , and density, ρ , further conditioned on abreast (Γ^{\leftrightarrow} , Eq 9) and in-file (Γ^{\uparrow} , Eq 10) dyads. In formulas, we consider the center of mass speeds for abreast and in-file configurations as

$$v_{\text{com}}^{\leftrightarrow, B}(\rho) = \mathbb{E}[v_{\text{com}} \mid (x_r, y_r) \in \Gamma^{\leftrightarrow}, \rho, B] \quad (21)$$

$$v_{\text{com}}^{\uparrow, B}(\rho) = \mathbb{E}[v_{\text{com}} \mid (x_r, y_r) \in \Gamma^{\uparrow}, \rho, B] \quad (22)$$

respectively. This fundamental diagram demonstrates that dyads consistently move slower than non-dyad pedestrians across all density conditions, corroborating previous findings from controlled laboratory experiments [7, 21] and smaller-scale empirical studies [29]. At low densities, abreast dyads move faster than in-file dyads, but this relationship reverses at higher densities ($\rho > 0.7 \text{ p/m}^2$), indicating a density-driven configuration transition. We hypothesize that in-file movement becomes more efficient for navigating crowded environments at higher densities, while in contrast it is known that at lower densities the abreast configuration is preferred to facilitate communication [30].

To quantify speed differences under uncongested conditions, Fig 6b compares free-flow speed distributions ($\mathbb{E}[v_{\text{com}} | B_{\text{free}}]$). Non-dyads show higher modal and mean speeds than dyads, with a 0.1 m/s modal difference, indicating slower dyad movement even in free flow. While this plot suggests that the modal speed may better reflect intrinsic velocity preferences, in we use the mean speed in our future analysis because, at higher densities, the distribution becomes bimodal with a secondary peak near the standing threshold v_s , complicating modal estimation.

We then examine how relative crowd motion modulates these relationships by analyzing mean speeds across the three dyad-crowd

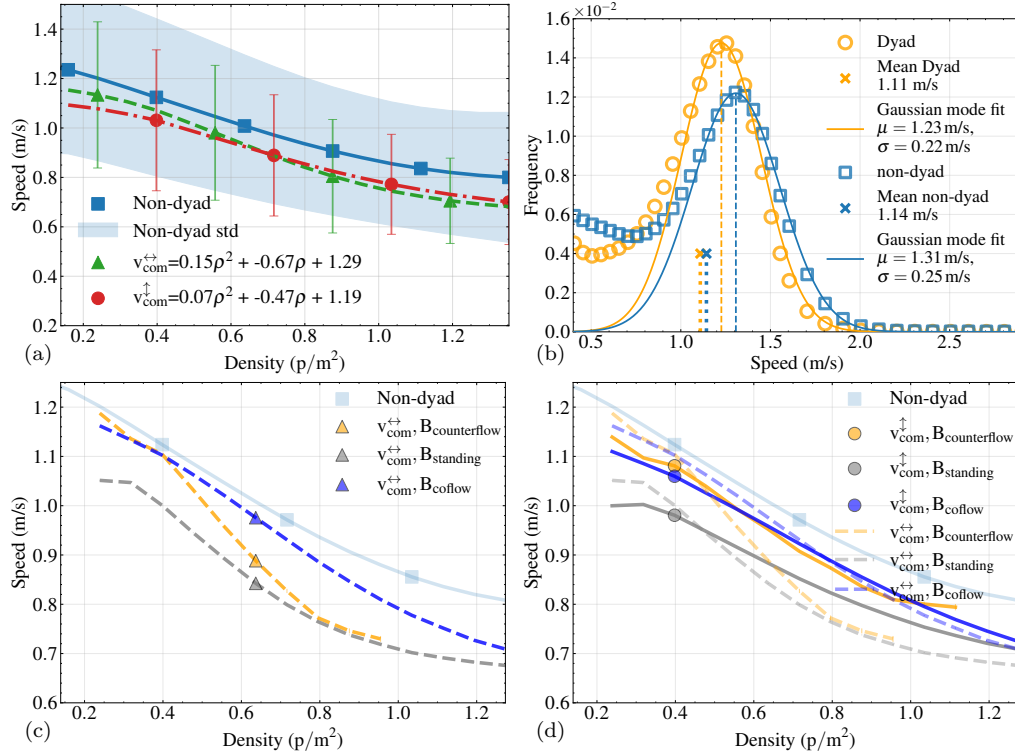


Fig 2. Dependency of dyad speed, v_{com} , on crowd density, ρ , for abreast (triangles) and in-file (circles) configurations. (a) Fundamental diagram ($\mathbb{E}[v_{com}|\rho, \mathbf{r}_{loc}]$): mean velocity and standard deviation vs. local density for non-dyad crowd members (blue squares), abreast dyads $v_{com}^{\leftrightarrow}$ (Eq 21, green triangles), and in-file dyads v_{com}^{\uparrow} (Eq 22, red circles). (b) Walking speed probability density in free-flow conditions ($\mathbb{E}[v_{com}|B_{\text{free}}]$) for dyad members (yellow circles) and non-dyad pedestrians (blue squares). Dashed vertical line: modal speed; dotted line with cross: mean speed; solid line: Gaussian fit to modal region. Both modal and mean speeds are slower for dyads vs. non-dyads. (c) Abreast dyad speeds conditioned on B Eq 14 ($\mathbb{E}[v_{com}|B, \rho]$). Note the different y-axis scale from (a). Co-moving dyads (B_{coflow} , dashed blue) maintain highest speeds, counter-flow dyads ($B_{\text{counterflow}}$, dashed yellow) intermediate speeds, and dyads in stationary crowds (B_{standing} , dashed gray) lowest speeds. (d) In-file dyad speeds (solid lines) across same B as in (c). The ordering of speeds among the different dyad types is the same as in (c). At low densities, in-file dyads are slower than abreast; this reverses at higher densities. Crossover occurs at $\rho \approx 0.5 \text{ p/m}^2$ for B_{standing} and $B_{\text{counterflow}}$, and at $\rho \approx 0.8 \text{ p/m}^2$ for B_{coflow} .

interaction regimes (Fig 6c-d). Both abreast and in-file configurations exhibit a consistent speed hierarchy across all densities: dyads co-moving with the crowd (B_{coflow}) maintain the highest speeds, those moving against the crowd ($B_{\text{counterflow}}$) achieve intermediate speeds, while dyads navigating through stationary crowds (B_{standing}) move slowest. This ordering is likely due to the increased navigational conflict between dyad and crowd:

- For B_{coflow} , dyads are likely to benefit from aligned flow direction, reducing navigational conflicts and enabling higher speeds dictated by the general crowd motion.
- For $B_{\text{counterflow}}$, they are expected to achieve intermediate speeds because both the dyad and oncoming pedestrians can actively adjust their trajectories to avoid conflict.

- In contrast, we hypothesize that for B_{standing} dyads must perform all adjustments themselves, resulting in the lowest speeds.

This ordering demonstrates that relative crowd motion, not density alone, fundamentally shapes dyad behavior. Moreover, Fig 6d reveals that the crossover density at which in-file becomes faster than abreast is regime-dependent: it occurs at $\rho \approx 0.5 \text{ p/m}^2$ for both B_{standing} and $B_{\text{counterflow}}$, but is at a substantially higher density of $\rho \approx 0.8 \text{ p/m}^2$ for B_{coflow} . We hypothesize that this regime-dependent transition may be attributed to how in-file configurations reduce navigational conflicts: when dyads traverse stationary crowds or move against the flow, the streamlined in-file arrangement becomes advantageous at lower densities due to the higher frequency of avoidance maneuvers required. In contrast, co-moving dyads experience fewer conflicts and can maintain the more comfortable abreast formation to higher densities before spatial constraints necessitate the transition to in-file.

Configuration heatmaps. To understand how dyads organize themselves during motion and under influence of the surrounding crowd, we examine their internal spatial configuration using the probability distribution of relative positions $\mathbb{P}(x_r, y_r)$. Specifically, we condition $\mathbb{P}(x_r, y_r)$ on speed and density, $\mathbb{P}(x_r, y_r | v_{\text{com}}, \rho)$ (Fig 3). The plots are arranged in a fundamental diagram format, with ρ increasing from left to right and v_{com} increasing from bottom to top. The heatmaps reveal two distinct most likely configuration states: abreast formations concentrated along the x_r axis and in-file formations along the y_r axis. At low densities, abreast configurations dominate across all speeds, while higher densities show increased probability of in-file arrangements. Moreover, this visualization shows the transition from predominantly abreast configurations at low densities (ρ_0 , left column), to a mixed configuration chance as density increases (ρ_2 , right column). This analysis, enabled by our unprecedented dataset scale, reveals for the first time the complete picture of density-driven configuration transitions: at low densities, abreast configurations dominate across all speed conditions, whereas at higher densities, in-file configurations become increasingly probable, though abreast formations remain present. The coexistence of both configuration indicates a need for additional conditioning to isolate more distinct regimes.

To better isolate the factors driving configuration transitions observed in Fig 3, we refine our analysis by conditioning on both density ρ and dyad-crowd interaction regimes B (Eq 14), examining $\mathbb{P}(x_r, y_r | B, \rho)$. This separates the effects of crowd density from those of relative motion direction and allows us to determine whether configuration changes are driven by more than just spatial constraints alone (i.e. ρ). In Fig 4 we present this analysis across three interaction regimes: B_{coflow} (co-moving, top row), B_{standing} (stationary crowd, middle row), and $B_{\text{counterflow}}$ (counter-flow, bottom row), each plotted across increasing density levels from left to right. This shows that in-file configurations become the relatively more likely than abreast configurations under specific conditions, specifically at higher densities when dyads traverse standing crowds (Fig 4f) or move against crowd flow (Fig 4j). Notably, at comparable density levels, dyads moving with the crowd maintain predominantly abreast configurations (Fig 4c), clearly distinguishing the configuration

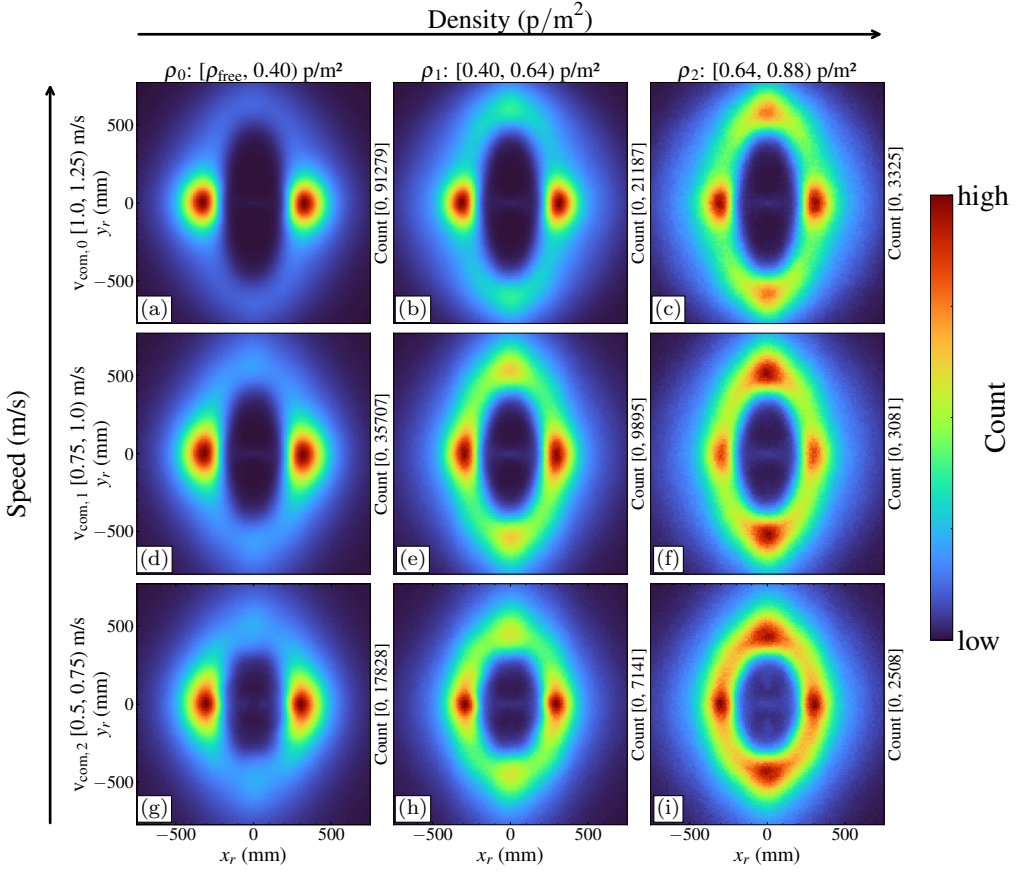


Fig 3. Probability density of dyad positions arranged in fundamental diagram format, showing how dyad configurations vary with density and speed. The colorization is scaled by the minimum and maximum values of the pdf indicated by Count[min, max] in each subplot. At low densities (left columns), abreast configurations near the x_r axis dominate across all speed bins (rows). As density increases, a secondary peak emerges near the y_r axis, corresponding to in-file configurations. This shift indicates that the likelihood of dyad configurations depends systematically on crowd density.

preferences that were mixed in Fig 3. This finding demonstrates that the direction of crowd-dyad interaction, not just density alone, is a key determinant of configuration transitions.

Relative position fundamental diagrams. Building on the previous configuration probability analysis (Fig 3, Fig 4), which revealed how dyad configurations vary with speed and density conditions, we now examine how these parameters vary spatially within the dyad's local coordinate frame. Inspired by the approach of [22] – whose results were limited by small sample sizes – we leverage on the scale of our dataset to quantify the typical conditions experienced at different relative positions through the conditional expectations $\mathbb{E}[\rho|\mathbf{r}_{loc}]$ (Fig 5a) and $\mathbb{E}[v_{com}|\mathbf{r}_{loc}]$ (Fig 5b).

The density-configuration relationship (Fig 5a) indicates that abreast configurations predominantly occur under lower-density conditions, whereas in-file configurations are associated with higher average densities. This is consistent with the previous result that at low density and higher speed (Fig 3a), the abreast configuration is most preferred. The

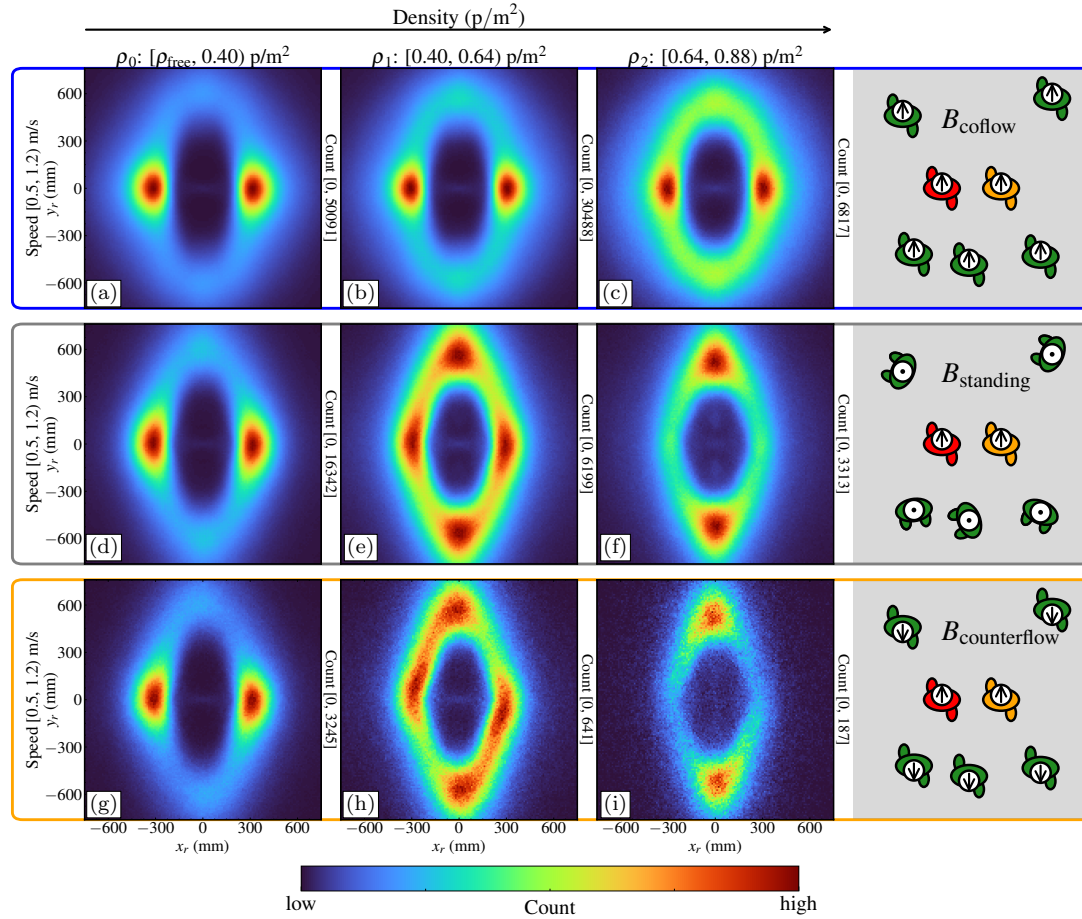


Fig 4. Probability density of dyad positions under different dyad-crowd interaction regimes B (Eq 14), showing how dyad configurations depend on relative crowd motion and density. Minimum and maximum values are indicated by Count[min, max] in each subplot. Top row: B_{coflow} (co-moving), middle row: B_{standing} (stationary crowd), bottom row: $B_{\text{counterflow}}$ (counter-flow). In contrast to Fig 3, this analysis shows that in-file configurations dominate at higher densities (right column) when dyads traverse standing crowds or move against the flow. At comparable densities, dyads moving with the crowd remain predominantly abreast, while those in standing or opposing crowds adopt in-file arrangements.

speed-configuration relationship (Fig 5b) shows a general trend: velocity decrease with smaller interpersonal distance. Additionally, Fig 5b reveals that dyads attain maximum average speeds (1.1 m/s) when positioned in abreast formations and minimum average speeds (0.7 m/s) in in-file formation. Examining this same regions in Fig 5a, shows that the regions of lower speeds coincide with areas of higher density, which is in line with the fundamental diagram Fig 6a. This suggests that elongated in-file configurations facilitate efficient movement through denser crowd environments.

Interpersonal distance analysis. To characterize the most likely dyad formations observed in Fig 3 and Fig 4, we analyze the mode of the interpersonal distance d_{ij} (i.e. the most frequent case) of both abreast and in-file dyads. We denote the modal distances for abreast and in-file dyads

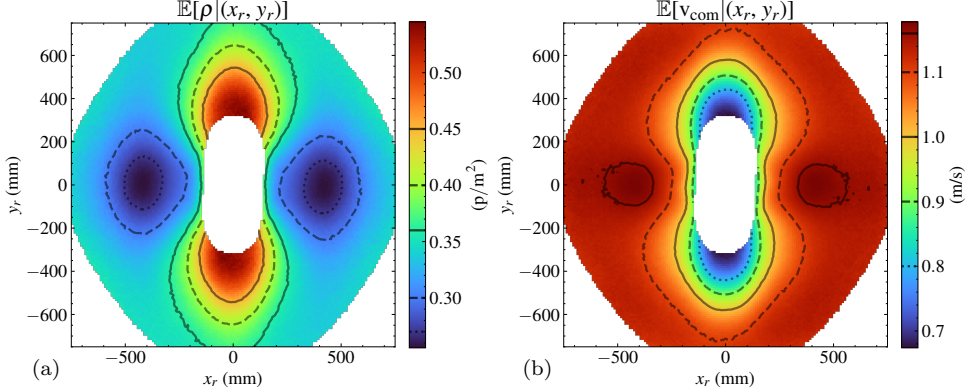


Fig 5. Dependence of density ρ and dyad speed v_{com} on the relative position \mathbf{r}_{loc} . (a) Density-configuration ($\mathbb{E}[\rho | (x_r, y_r)]$) diagram indicating that abreast configurations occur predominantly at lower ρ than in-file configurations. (b) Speed-configuration ($\mathbb{E}[v_{\text{com}} | (x_r, y_r)]$) diagram showing that smaller interpersonal distances correspond to lower speeds in both configurations, with a stronger effect for in-file dyads. The highest expected v_{com} is observed in a concentrated region centered along the y_r axis.

by D^{\leftrightarrow} and D^{\dagger} , respectively. Operationally, the D is calculated by extracting the most common distances from the probability distributions $\mathbb{P}(x_r, y_r | \rho)$ by integrating over narrow bands around each principal axis, as detailed in Appendix B. Gaussian fits to the resulting marginal distributions yield the modal position μ and standard deviation σ , from which we define D as:

$$D^{\leftrightarrow} = 2\mu^{\leftrightarrow}, \quad D^{\dagger} = 2\mu^{\dagger}, \quad \sigma_D^{\leftrightarrow} = 2\sigma^{\leftrightarrow}, \quad \sigma_D^{\dagger} = 2\sigma^{\dagger}. \quad (23)$$

In Fig 6, we present the relationship between these modal interpersonal distances D and local density ρ .

The relationship between interpersonal distance and density reveals an asymmetric response between configurations. For abreast dyads (D^{\leftrightarrow}), the interpersonal distance remains relatively stable across low to moderate densities, declining only slightly from approximately 0.7 m, before plateauing asymptotically at $D^{\leftrightarrow} \approx 0.6$ m for higher densities. This plateau likely reflects a minimum comfortable side-by-side distance constrained by body width and personal space requirements. In contrast, in-file dyads (D^{\dagger}) exhibit a sharp, continuous decrease in interpersonal distance with increasing density, declining from approximately 1.30 m at $\rho = 0.2 \text{ p/m}^2$ to 0.95 m at $\rho = 1.0 \text{ p/m}^2$. This asymmetric compressibility likely reflects the different biomechanical constraints in each configuration: in-file dyads can reduce their longitudinal spacing by adjusting their gait phase and stride length to avoid stepping on each other's heels, while abreast dyads face a hard lower bound set by shoulder width and the physical impossibility of occupying the same lateral space. This demonstrates that spatial constraints imposed by crowd density affect the two abreast and in-file configurations differently.

2.2 Orientation Log-Odds, Π_{OLO} : scalar reduction of dyad configuration

In Section 2.1, we showed how crowd density and flow regime, together with the dyad velocity, determine systematic changes in the

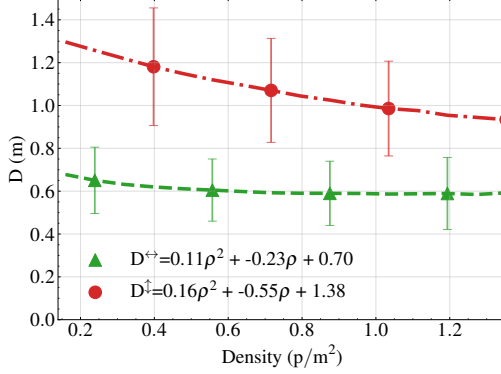


Fig 6. Modal interpersonal distances (D) and their standard deviations as a function of local density ρ for abreast (green triangles, D^{\leftrightarrow}) and in-file (red circles, D^{\uparrow}) dyads. Abreast configurations show a slight decline that flattens asymptotically at $D^{\leftrightarrow} \approx 0.6$ m, while in-file configurations exhibit a continuous decreasing trend throughout the density range.

probability of the dyad spatial configuration. Here, we obtain a compact, interpretable measure of the dyad configuration: we reduce the 2D probability distribution $\mathbb{P}(x_r, y_r | \boldsymbol{\theta})$, with $\boldsymbol{\theta}$ indicating some generic state parameter, to a single scalar reflecting the relative probability of the dyad being in the abreast versus the in-file state. This will unlock a quantitative analysis and modeling of the probabilistic dependency of the dyad formation on different choices of $\boldsymbol{\theta}$ (Section 3). Specifically, we coarse grain our observation considering the probability of being within abreast (Γ^{\leftrightarrow} , Eq 9) or in-file (Γ^{\uparrow} , Eq 10) configurations. This establishes, respectively, the two complementary conditional Bernoulli probabilities

$$\mathbb{P}(\Gamma^{\uparrow} | \boldsymbol{\theta}) = \int_{\Gamma^{\uparrow}} d\mathbb{P}(x_r, y_r | \boldsymbol{\theta}) \quad \text{in-file probability,} \quad (24)$$

$$\mathbb{P}(\Gamma^{\leftrightarrow} | \boldsymbol{\theta}) = \int_{\Gamma^{\leftrightarrow}} d\mathbb{P}(x_r, y_r | \boldsymbol{\theta}) \quad \text{abreast probability.} \quad (25)$$

These two probabilities are linked to each other by the relation

$$\mathbb{P}(\Gamma^{\leftrightarrow} | \boldsymbol{\theta}) + \mathbb{P}(\Gamma^{\uparrow} | \boldsymbol{\theta}) = 1, \quad (26)$$

which follows from the fact that Γ^{\leftrightarrow} and Γ^{\uparrow} are a disjoint partition of the (x_r, y_r) plane.

Finally, we introduce scalar quantity, dependent on and equivalent to $\mathbb{P}(\Gamma^{\leftrightarrow} | \boldsymbol{\theta})$, but with additional interpretability and geometric features. We dub it Orientation Log-Odds (OLO), Π_{OLO} , and in formulas it reads:

$$\Pi_{\text{OLO}}(\boldsymbol{\theta}) = \log_2 \frac{\mathbb{P}(\Gamma^{\leftrightarrow} | \boldsymbol{\theta})}{\mathbb{P}(\Gamma^{\uparrow} | \boldsymbol{\theta})} = \text{logit}_2(\mathbb{P}(\Gamma^{\leftrightarrow} | \boldsymbol{\theta})). \quad (27)$$

Π_{OLO} comes with three useful properties:

1. it quantifies the relative likelihood of abreast ($\Pi_{\text{OLO}} > 0$) versus in-file ($\Pi_{\text{OLO}} < 0$) configurations, with $\Pi_{\text{OLO}} = 0$ indicating equal probability for both states (cf. examples in Fig 7). Any additional OLO unit implies the abreast configuration been twice more likely than the in-file case (due to the \log_2 base choice).

2. It reflects the symmetry of our definition of the regions Γ^{\leftrightarrow} and $\Gamma^{\uparrow\downarrow}$ that are identical up to a 90° rotation of the (x_r, y_r) plane with a sign shift:

$$\Gamma^{\leftrightarrow} \xrightarrow{\text{Rot}_{90}} \Gamma^{\uparrow\downarrow} \quad (28)$$

$$(x_r, y_r) \xrightarrow{\text{Rot}_{90}} (\mp y_r, \pm x_r) \quad (29)$$

$$\Pi_{\text{OLO}} \xrightarrow{\text{Rot}_{90}} -\Pi_{\text{OLO}} \quad (30)$$

3. The Π_{OLO} can be interpreted as the difference in (dimensionless) energy between the two states under a Boltzmann-like distribution ($\mathbb{P}(x) \propto e^{+E(x)}$ for a generic state x with energy $E(x)$):

$$\Pi_{\text{OLO}} = \log_2 \frac{\mathbb{P}(\Gamma^{\leftrightarrow})}{\mathbb{P}(\Gamma^{\uparrow\downarrow})} \propto (E_{\Gamma^{\uparrow\downarrow}} - E_{\Gamma^{\leftrightarrow}}), \quad (31)$$

where $E_{\Gamma^{\uparrow\downarrow}}$ and $E_{\Gamma^{\leftrightarrow}}$ are respectively the energies of the in-file and abreast states. Such an interpretation aligns with the Langevin-like approaches that have been extensively used to model pedestrian dynamics [3].

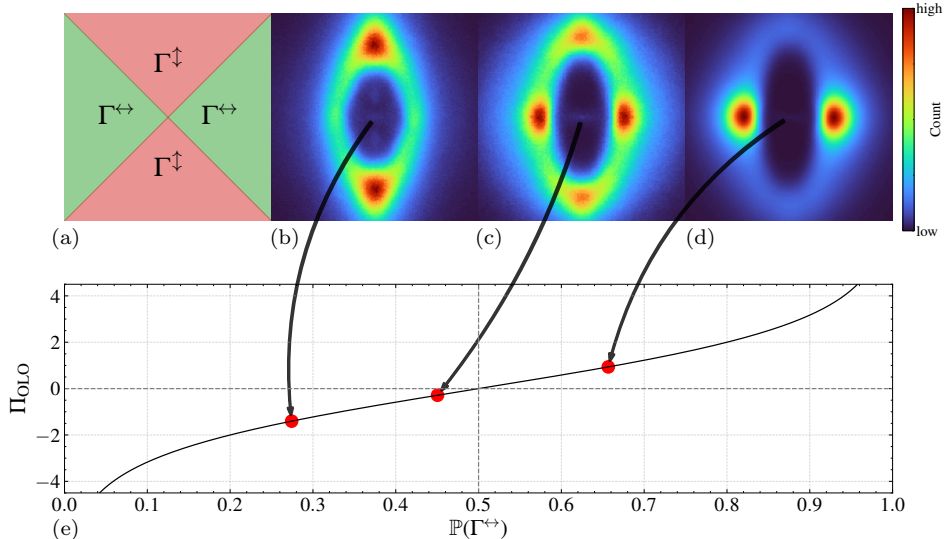


Fig 7. Values of Π_{OLO} (Eq 27), i.e., relative probability of abreast versus in-file configurations, for different probability density of dyad positions. (a) Division of the (x_r, y_r) plane into abreast states Γ^{\leftrightarrow} (green, Eq 9) and in-file states $\Gamma^{\uparrow\downarrow}$ (red, Eq 10). (b-d) Example probability density for dyads in different regimes: (b) in-file states dominate ($\Pi_{\text{OLO}} \approx -1 < 0$), (c) in-file and abreast are equally likely ($\Pi_{\text{OLO}} \approx 0$), and (d) abreast states dominate ($\Pi_{\text{OLO}} \approx 1 > 0$). (e) Π_{OLO} as a function of the probability an abreast state $\mathbb{P}(\Gamma^{\leftrightarrow})$.

3 Π_{OLO} and dyad formation in dependence on crowd conditions

Here we examine in probabilistic terms how the dyad formation changes in dependence of the surrounding crowd state. We leverage on the synthetic indicator Π_{OLO} (Eq 27), which we characterize in dependence of crowd

density ρ , dyad speed, v_{com} , flow regime B (Eq 14), and relative speed $\tilde{v}_{||}$ (Eq 15), which we will synthetically refer to with the vector parameter $\boldsymbol{\theta}$. Specifically, we model the relation

$$\Pi_{\text{OLO}} = \Pi_{\text{OLO}}(\rho, v_{\text{com}}, B, \tilde{v}_{||}) = \Pi_{\text{OLO}}(\boldsymbol{\theta}). \quad (32)$$

We consider three regimes of increasing complexity with underlying modeling assumption that in the absence of nearby pedestrians, dyads follow some intrinsic “free-flow” dynamics that are perturbed by the presence of a crowd. Specifically, these regimes are (1) free-flow conditions (B_{free}), (2) dyads moving through stationary crowds (B_{standing}), (3) and, finally, the general dynamic conditions in which both dyad and crowd move in co- or counter- flow. In each of these regimes, some components of $\boldsymbol{\theta}$ vanish or are set to specific values, which we will clarify by writing a conditioning statement, e.g.,

$$(\boldsymbol{\theta} \mid B = B_{\text{free}}), \quad (33)$$

to mean that only parameters relevant in free-flow are active in the parameter vector $\boldsymbol{\theta}$.

3.1 Π_{OLO} in free flow regime, B_{free}

By our definition of free flow regime, B_{free} (Eq 14), there is no crowd nearby the dyad, hence, the variables ρ and \mathbf{v}_{prox} carry no effect on the dyad formation. Consequently, Π_{OLO} only depend on the dyad speed v_{com} , i.e., in formulas

$$\Pi_{\text{OLO}}(\boldsymbol{\theta} \mid B = B_{\text{free}}) = \Pi_{\text{OLO}}^{\text{free}}(v_{\text{com}}) \quad (34)$$

In Fig 8a, we report the measured values $\Pi_{\text{OLO}}^{\text{free}} = \Pi_{\text{OLO}}^{\text{free}}(v_{\text{com}})$. We observe that $\Pi_{\text{OLO}}^{\text{free}}$ is strictly positive and, in particular,

$$\Pi_{\text{OLO}}^{\text{free}}(v_{\text{com}}) \geq 0.65 > 0 \quad \forall v_{\text{com}} \in [0.5, 1.75] \text{ m/s}. \quad (35)$$

Hence, in line with previous findings [5, 30], the abreast configuration is always more likely than the in-file configuration - indeed by a factor $\approx 2^{0.65} \approx 1.57$ or larger. Moreover, $\Pi_{\text{OLO}}^{\text{free}}$ depends on speed in a non-monotonic way, and we can isolate two critical velocity values:

$$v_L \approx 0.70 \text{ m/s} \quad \Pi_{\text{OLO}}^{\text{free}}(v_{\text{com}}) \approx 0.65 \quad v_{\text{com}} \leq v_L \quad \text{minimum} \quad (36)$$

$$v_H \approx 1.35 \text{ m/s} \quad \Pi_{\text{OLO}}^{\text{free}}(v_H) \approx 1.9 \quad \text{relative maximum}. \quad (37)$$

Note that v_L and v_H are, respectively, smaller and larger than the free flow modal speed ($\mu_{\text{dyad}} = 1.23 \text{ m/s}$, Fig 6b); moreover, at $v_{\text{com}} = v_H$, abreast configurations are almost four times more likely than in-file cases.

We conjecture that these formations reflect the dyad’s certainty regarding its movement goal and the urgency to reach this goal:

- at low speeds ($v_{\text{com}} \approx v_L$), uncertainty about the destination may result in less structured configurations;
- at moderate speeds ($v_L < v_{\text{com}} < v_H$), increased speed may indicate greater goal clarity, shifting the focus toward communication and comfort [30], which is facilitated by abreast formations;

- at high speeds ($v_{\text{com}} > v_H$), as the dyad enters the running regime, the movement is likely driven by urgency, and efficient movement becomes the priority. This reduces the likelihood of abreast configurations due to potential speed mismatches between members.

The non-monotonic trend of Π_{OLO} is a strong feature that extends beyond the free flow regime, and it is the central element in our model. In particular, the simplest model featuring a relative minimum and maximum satisfies

$$\frac{\partial \Pi_{\text{OLO}}^{\text{free}}(v_{\text{com}})}{\partial v_{\text{com}}} \propto -(v_{\text{com}} - v_L)(v_{\text{com}} - v_H), \quad (38)$$

which, up to a scaling factor $A > 0$ and an offset E , gives (cf. dotted line in Fig 8a)

$$\Pi_{\text{OLO}}^{\text{free}}(v_{\text{com}}) = -A \left(\frac{v_{\text{com}}^3}{3} - \frac{v_{\text{com}}^2}{2}(v_L + v_H) + v_{\text{com}} v_L v_H \right) + E. \quad (39)$$

This simple polynomial model matches the data accurately between 0.5 m/s and 1.6 m/s, while fails at velocities higher than 1.6 m/s (very rare), since the measured $\Pi_{\text{OLO}}^{\text{free}}(v_{\text{com}})$ has a slower decay and likely no zero-crossing (i.e. we expect that at high velocity dyads have no reason to move switch to a prominently in-file configuration).

3.2 Π_{OLO} in static crowd conditions, B_{standing}

In comparison with the free flow regime, the case of a dyad walking through a standing crowd adds the additional crowd density parameter, ρ , to the system. In formulas, we now consider the relation

$$\Pi_{\text{OLO}}(\theta | B = B_{\text{standing}}) = \Pi_{\text{OLO}}^{\text{standing}}(\rho, v_{\text{com}}), \quad (40)$$

which we report for five selected density levels in Fig 8b and in terms of contours in Fig 8c. The phenomenology is quite rich, and has the following features:

- for density levels

$$\rho < 1.05 \text{ p/m}^2 =: \rho_T, \quad (41)$$

Π_{OLO} decreases with ρ : higher density yields a general preference towards in-file.

Moreover, regardless the speed v_{com} , at density

$$\rho > 0.35 \text{ p/m}^2 =: \rho_C \quad (42)$$

the in-file configuration is always preferred. This holds even up to a ten-fold factor around the state ($v_{\text{com}} = 1.2 \text{ m/s}$, $\rho = \rho_T$). We hypothesize that this trend arises from the fact that in-file configurations enable easier navigation through a crowd.

Conversely, when $\rho > \rho_T$, $\Pi_{\text{OLO}}^{\text{standing}}$ increases slightly with density, though remaining negative (in-file dominates). We hypothesize that at high densities, the dyad's agency diminishes, and configuration is increasingly dictated by crowd conditions rather than individual preference;

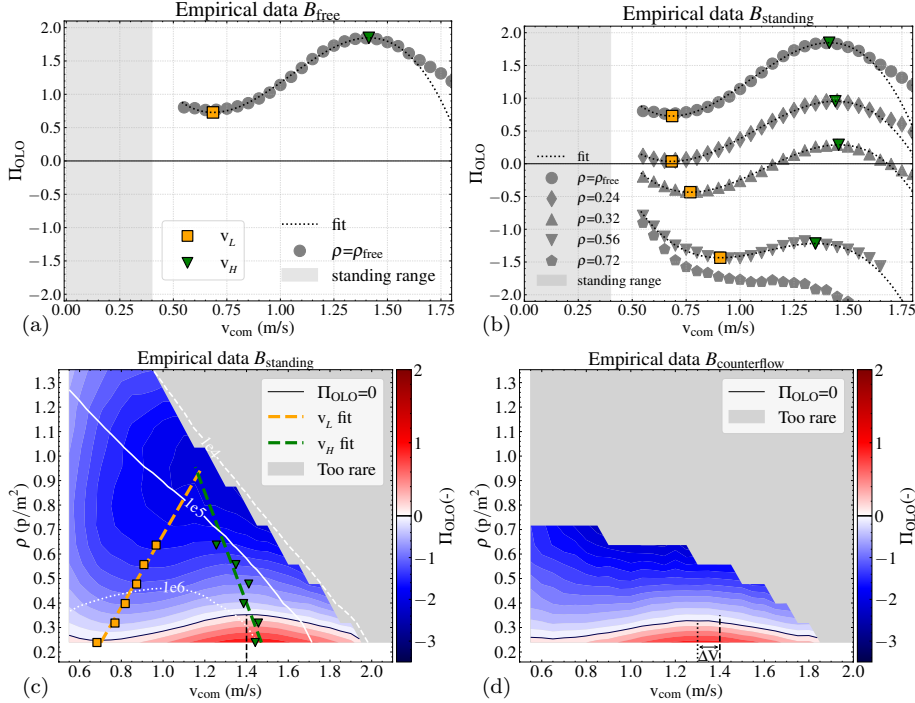


Fig 8. Π_{OLO} as a function dyad speed v_{com} for (a) a dyad in free-flow conditions B_{free} , (b,c) a dyad traversing a standing crowd B_{standing} and (d) a dyad going against a crowd $B_{\text{counterflow}}$. The dyad configuration preference changes with dyad speed v_{com} and density ρ . (a) In B_{free} conditions, Π_{OLO} varies non-monotonically with v_{com} , showing a minimum at v_L and a maximum at v_H , with $\Pi_{\text{OLO}} > 0$ throughout (i.e., $\mathbb{P}(\Gamma^{\leftrightarrow}) > \mathbb{P}(\Gamma^{\dagger})$, abreast more likely). (b) In B_{standing} conditions, the overall shape of Π_{OLO} is preserved and systematically decreases as ρ increases: higher densities promote in-file configurations ($\Pi_{\text{OLO}} < 0$). (c) Contour plot of the standing-crowd condition across all recorded densities, showing that velocities v_L and v_H approach one-another, meeting at finite density (linear fits). The black contour line marks $\Pi_{\text{OLO}} = 0$ ($\mathbb{P}(\Gamma^{\leftrightarrow}) = \mathbb{P}(\Gamma^{\dagger})$). (d) Contour plot for the opposing-crowd condition, $B_{\text{counterflow}}$ exhibiting similar behavior to (c). Note that the counter-flow regime Π_{OLO} trend can be obtained from the standing flow case with good accuracy via a rescaling and translation transformation (see Section 3.3). In (c-d) the black contour line marks the $\Pi_{\text{OLO}} = 0$ abreast-in-file transition ($\mathbb{P}(\Gamma^{\leftrightarrow}) = \mathbb{P}(\Gamma^{\dagger})$); gray regions denote insufficient data (less than 10^4 data points - in panel (c), contours outlining amount of data in different regions are in white).

- at all observed densities, $\Pi_{\text{OLO}}^{\text{standing}}$ is systematically closest to zero at the lowest velocity levels considered ($v_{\text{com}} \approx 0.5 \text{ m/s}$). In other terms, at lower velocities there is higher uncertainty about the preferred configuration of a dyad, e.g. due to uncertainty in destination, as mentioned in the free-flow case;
- increasing ρ from the free-flow regime, when $\rho = 0.32 \text{ p/m}^2 = \rho_c$, $\Pi_{\text{OLO}}^{\text{standing}}$ crosses zero for the first time: the abreast configurations become as likely as the in-file. At even higher density levels, abreast states become increasingly less likely than in-file configurations. Moreover, at $\rho = \rho_c$ when a dyad walks at velocity $v_{\text{com}} \approx 0.75 \text{ m/s} (= v_L)$ the in-file configuration is about 1.4 times more likely than the abreast. Such a likelihood completely reverses at $v_{\text{com}} \approx 1.4 \text{ m/s} (= v_H)$;
- the non-monotonic dependency of Π_{OLO} on v_{com} observed in the

free-flow case extends to the standing case, up to $\rho \approx 0.7 \text{ p/m}^2$. We have two critical velocities, $v_L = v_L(\rho)$ and $v_H = v_H(\rho)$, at which the likelihood of abreast configurations remains, respectively lowest and highest (marked, respectively, with green squares and green triangles in Fig 8a-c).

The distance $|v_H - v_L|$ diminishes as the density increases.

Effectively, at $\rho \approx 0.7 \text{ p/m}^2$, $\Pi_{\text{OLO}}^{\text{standing}}$ has a saddle-node-like bifurcation and its critical points disappear, acquiring a monotonically decreasing behavior;

- in the (v_{com}, ρ) plane, not all the states are possible. High density conditions for which also v_{com} is high are unlikely. This translates to the gray-shaded region in Fig 8c, that marks cases that are physically impossible or very unlikely (less than ≈ 10.000 measurements). The boundary of these impossible/unlikely conditions satisfies $\partial\rho/\partial v_{\text{com}} < 0$, signaling, as expected that the maximum feasible speed through a crowd diminishes with density. This is likely due to increased physical constraints and reduced maneuverability.

We model $\Pi_{\text{OLO}}^{\text{standing}}$ by generalizing $\Pi_{\text{OLO}}^{\text{free}}$ (Eq 39). Primarily, we allow v_L , v_H to depend linearly on the density, say

$$v_H(\rho) = \alpha_h \rho + \beta_h \quad v_L(\rho) = \alpha_l \rho + \beta_l, \quad (43)$$

with parameters identified through linear fits of the fundamental diagrams $v_L = v_L(\rho)$ and $v_H = v_H(\rho)$. Note that this means that $\partial\Pi_{\text{OLO}}^{\text{standing}}/\partial v_{\text{com}}$ scales as the product of two fundamental diagrams. After integration, this gives

$$\Pi_{\text{OLO}}^{\text{standing}}(v_{\text{com}}, \rho) = -A \left(\frac{v_{\text{com}}^3}{3} - \frac{v_{\text{com}}^2}{2} (v_L(\rho) + v_H(\rho)) + v_{\text{com}} v_L(\rho) v_H(\rho) \right) + E, \quad (44)$$

Note that a more accurate fit could be obtained by allowing also linear dependence of the multiplying factor A on the density

$$A = A(\rho) = \alpha_A \rho + \beta_A; \quad (45)$$

this increased complexity nevertheless contributes only a $\approx 5\%$ variation (cf. values in Tab. 1a).

This simple model of the Π_{OLO} behavior in the standing regime has a very good agreement with the measurements: in Fig 9a we report the contour plot yielded by the model, which recover all the qualitative features observed above. For a quantitative assessment, in Fig 9c we report the absolute error (AE) between predicted and empirical Π_{OLO} values ($\text{AE}(v_{\text{com}}, \rho) = |(\Pi_{\text{OLO}}^{\text{model}}(v_{\text{com}}, \rho) - \Pi_{\text{OLO}}^{\text{data}}(v_{\text{com}}, \rho))|$), which showcases how the model is accurate up to $v_{\text{com}} \approx 1.7 \text{ m/s}$ and densities up to 1.1 p/m^2 . Appendix C includes an empiric equation (Eq 53) for the region in the (v_{com}, ρ) plane in which our model is defined.

3.3 Π_{OLO} in generic flow conditions

We relax here the previous regime constraints, and we look at Π_{OLO} in generic co-flow and counter-flow conditions. The formation behavior in co- and counter- flow conditions changes quite dramatically. To showcase it, we proxy first the flow regime using the relative parallel velocity variable,

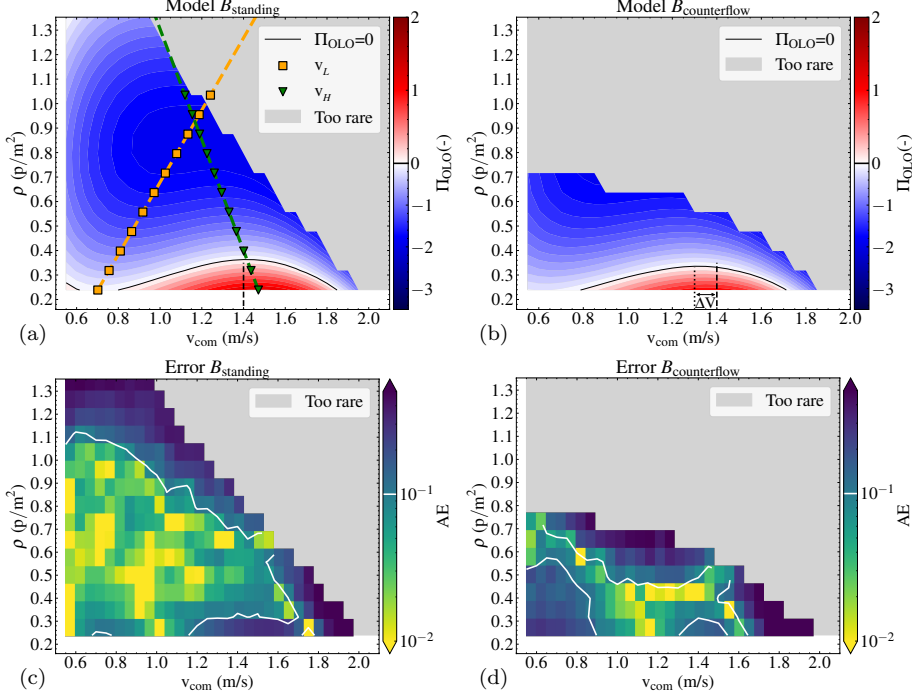


Fig 9. Contour plots of Π_{OLO} (Eq 27) models for standing B_{standing} (Eq 44) and counter-flow $B_{\text{counterflow}}$ (Eq 50) conditions. (a) Standing crowd model showing polynomial-like structure with characteristic velocities $v_L(\rho)$ and $v_H(\rho)$ that converge as density increases toward $\rho_T = 1.05 \text{ p/m}^2$. (b) Counter-flow model obtained by applying velocity offset $\Delta V = 0.1 \text{ m/s}$ and density compression $Z = 1.08$ to the standing case (Eq 50), exhibiting similar functional form but shifted to lower velocities and compressed density range. In (a-b) the black contour line marks $\Pi_{\text{OLO}} = 0$, i.e., $\mathbb{P}(\Gamma^{\leftrightarrow}) = \mathbb{P}(\Gamma^{\uparrow})$, and gray regions indicate insufficient data (less than 10^4 measurements). (c) Absolute error (AE) between model (a) and empirical data (Fig 8c), demonstrating good predictive accuracy for $v_{\text{com}} < 1.7 \text{ m/s}$ and $\rho < 1.1 \text{ p/m}^2$. (d) Absolute error between model (b) and empirical data (Fig 8d), showing accurate predictions for $v_{\text{com}} < 1.6 \text{ m/s}$. Deviations in both models occur primarily at domain edges and rare high-velocity conditions.

Symbol	Value	Units
α_l	0.68	$\text{m}^3 \text{s}^{-1} \text{p}^{-1}$
β_l	0.54	m s^{-1}
α_h	-0.44	$\text{m}^3 \text{s}^{-1} \text{p}^{-1}$
β_h	1.58	m s^{-1}
α_A	1.34	$\text{m}^{-1} \text{s}^3 \text{p}^{-1}$
β_A	2.22	$\text{m}^{-3} \text{s}^3$
E	5.10	-

Table 1. Parameters of our model for $\Pi_{\text{OLO}}^{\text{standing}}(v_{\text{com}}, \rho)$ (Eq 44).

$\tilde{v}_{||}$ (Eq 15). In Fig 10, we report the contours of Π_{OLO} in dependency of the relative parallel velocity and density, i.e. of the relation

$$\Pi_{\text{OLO}}(\boldsymbol{\theta} \mid \forall v_{\text{com}}, \forall B) = \hat{\Pi}_{\text{OLO}}(\rho, \tilde{v}_{||}). \quad (46)$$

We can observe substantially different behaviors

- in counter-flow conditions ($\tilde{v}_{||} < 0$),
the density $\rho \approx \rho_C$ (Eq 42) marks the $\hat{\Pi}_{\text{OLO}} = 0$ threshold line, with

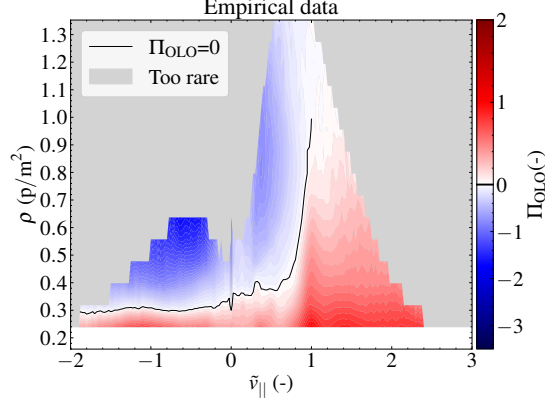


Fig 10. $\hat{\Pi}_{\text{OLO}}$ as a function of local density ρ and relative parallel velocity \tilde{v}_{\parallel} (cf. Eq 15, Eq 15), showing configuration preferences for $B_{\text{counterflow}}$ ($\tilde{v}_{\parallel} < 0$) and B_{coflow} ($\tilde{v}_{\parallel} > 0$). Three distinct behavioral regimes are evident: (i) Counter-flow conditions ($\tilde{v}_{\parallel} < 0$) show density-dependent transitions with minimal velocity dependence, similar to the standing crowd case; (ii) Co-flow with dyad overtaking crowd ($0 < \tilde{v}_{\parallel} < 1$) exhibits a sharp transition from counter-flow-like behavior to abreast preference; (iii) Co-flow with crowd overtaking dyad ($\tilde{v}_{\parallel} > 1$) shows strong abreast preference that decreases with density. The black contour line marks $\hat{\Pi}_{\text{OLO}} = 0$ ($\mathbb{P}(\Gamma^{\leftrightarrow}) = \mathbb{P}(\Gamma^{\dagger})$). Gray regions denote insufficient data.

practically no dependency on the relative velocity \tilde{v}_{\parallel} . In other terms, the transition density, already observed for the standing case, extends to the counter-flow case. We will conclude this section showing examining the counter-flow case in higher detail and showing how our Π_{OLO} model for standing crowd extends up to constant shift in this regime.

- the co-flow case ($\tilde{v}_{\parallel} > 0$) features two sub-cases, indeed sharply marked by the almost asymptotic behavior of the threshold line $\Pi_{\text{OLO}} = 0$ around the speed-matching conditions $\tilde{v}_{\parallel} \approx 1$:

$$\frac{\partial \rho}{\partial \tilde{v}_{\parallel}} \Big|_{\hat{\Pi}_{\text{OLO}}=0, \tilde{v}_{\parallel}=1} \gg 1. \quad (47)$$

For a dyad co-flowing and been overtaken by the surrounding crowd we have preference for abreast conditions:

$$\hat{\Pi}_{\text{OLO}} \left(\tilde{v}_{\parallel} > 1, \rho < 1 \text{ p/m}^2 \right) > 0 \quad (48)$$

Such a preference decreases with density and as we approach $\rho \approx 1 \text{ p/m}^2$, uncertainty in formation ($\hat{\Pi}_{\text{OLO}} \approx 0$) is highest. We interpret this as follows: when the dyad is being overtaken by the crowd, it is likely within a leisure walking condition and the abreast configuration is favored e.g. to allow interactions. Such “relaxed” abreast state becomes however harder and harder to maintain with density. Moreover, cases with high density and high relative velocity are clearly unlikely to happen as represented by the gray-shaded areas marking insufficient measurements;

- in case of dyad overtaking the crowd ($0 < \tilde{v}_{\parallel} < 1$), $\hat{\Pi}_{\text{OLO}}$ shows a sharp transition between the density-independent counter-flow-like regime in which in-file configurations are preferred past a critical

density, and the abreast-dominated behavior beyond the speed-matching condition. Note that, as commented after Eq 15, $\tilde{v}_{||} \approx 0^+$ is a case only possible when the dyad walks much faster than the surrounding crowd, which, might effectively appear to the dyad as standing.

3.3.1 Π_{OLO} in counter-flow crowd conditions, $B_{\text{counterflow}}$

We conclude analyzing and model the final regime, $B_{\text{counterflow}}$, in which the dyad is moving against a crowd. As shown in Fig 10, we can neglect in first instance the role of $\tilde{v}_{||}$, thus we consider the dependency

$$\Pi_{\text{OLO}}(\boldsymbol{\theta} \mid B = B_{\text{counterflow}}, \forall \tilde{v}_{||}) = \Pi_{\text{OLO}}^{\text{counterflow}}(v_{\text{com}}, \rho), \quad (49)$$

whose contours we report in Fig 8d. Notably, $\Pi_{\text{OLO}}^{\text{counterflow}}$ exhibits a similar functional form to $\Pi_{\text{OLO}}^{\text{standing}}$ (Fig 8c), i.e. dyads exhibit similar behavior, while crossing a standing or a counter-flowing crowd, yet with minor differences:

- all previously observed features from the B_{standing} regime (see Section 3.2) are slightly compressed in the ρ direction ($1/Z = 1/1.08$) and occur at slightly lower velocities ($-\Delta V = -0.1 \text{ m/s}$) and in the $B_{\text{counterflow}}$ scenario. This is likely due to increased navigational complexity, which reduces the overall traversal speed of dyads and decreases the velocity range where the previous behaviors emerge. While compression along the density axis may indicate that dyads perceive counter-flowing crowds as effectively denser than stationary ones;
- the region with insufficient data is notably larger, with no observations for $\rho > 0.8 \text{ p/m}^2$. This likely indicates that dyads tend to avoid moving against a crowd beyond this density threshold.

Due to the structural similarities, we prioritize interpretable, low-parameter models and base our model for $\Pi_{\text{OLO}}^{\text{counterflow}}$ on the standing-crowd case $\Pi_{\text{OLO}}^{\text{standing}}$ (Eq 44):

$$\Pi_{\text{OLO}}^{\text{counterflow}}(v_{\text{com}}, \rho) = \Pi_{\text{OLO}}^{\text{standing}}(v_{\text{com}} + \Delta V, Z \rho), \quad (50)$$

where ΔV represents the effective velocity offset, and Z the effective compression induced by opposing crowd flow. The contour plot resulting from the model is depicted in Fig 9b. As shown in Fig 9d, the model achieves low AE and closely matches the observed transition lines and main trends. Deviations are mainly found at the edges of the domain, higher velocities ($> 1.6 \text{ m/s}$) and ($> 0.6 \text{ p/m}^2$). Appendix C includes an empiric equation (Eq 54) for the region in the (v_{com}, ρ) plane in which our model is defined.

4 Discussion

In this paper, we presented a large-scale probabilistic analysis of the dynamics of dyads, i.e. groups of two pedestrians, walking in real-world crowded environments. We leveraged on a multi-year anonymous pedestrian trajectory dataset from Eindhoven Central Station (NL), in

which we automatically identified over $6M$ dyads. Given the anonymity constraint, our dataset included only position features and tracking (i.e. no orientation or any further kinematic or personal feature). To automate the dyad identification process we relied on proxemics heuristics (distance consistency) and leveraged on a previously proposed graph-based approach. The dyad dataset that we have established is several orders of magnitude larger than currently used, unlocking robust conditional analyzes of both average behavior and fluctuations in dyad dynamics.

At the core of our work is a collection of probabilistic phenomenological relations that connect the dynamics of dyads and those of the surrounding crowds in terms of kinematic observables. Such observables are the dyad center of mass speed, its spatial formation, the crowd density in the neighborhood of the dyad, and the crowd relative velocity. On these bases, we employed a large collection of quantities that can be deterministically derived from these observables. With data anonymity in mind, we argue that these provide a minimal, yet practically exhaustive, family of relevant observables.

Our probabilistic analysis provides a thorough phenomenological description of dyads, supplying a collection of fundamental diagram-like notions. Throughout our work, we analyzed finer and finer aspects of the dynamics of dyads, starting indeed from traditional fundamental diagrams, i.e., density-speed relations. Regardless of the specific flow condition, dyads move $\approx 10\%$ slower than a generic pedestrian in a crowd for comparable macroscopic density. Also, regardless of the specific flow condition, we observe that dyads in abreast configuration move faster than in-file for low density, and this trend is reversed in high density. The specific cross-over density is flow-regime dependent. As one could expect, the cross-over occurs at lower density ($\rho \approx 0.5 \text{ p/m}^2$) for counter-flowing and standing crowds, compared to co-flowing crowds ($\rho \approx 0.8 \text{ p/m}^2$). Dyads in counter-flow also move substantially slower than dyads in co-flow by at least 10%.

The relevant phenomenology of dyads extends however beyond the velocity of the center of mass, since the degrees of freedom include a “rotational” component and a relative distance component. At low density, dyads are most likely observed in abreast configuration. This holds robustly until density levels of $0.3 - 0.4 \text{ p/m}^2$. The rotational degree of freedom is enabled by increasing the dyad velocity and/or surrounding density, with this process being enhanced when the dyad is in counter-flow or when walks through a standing crowd (in opposition to the co-flow case). The distance between the dyad pair also has a dependency on the density. Yet, we observe that the distance in abreast configuration to be almost density independent (modal abreast distance $\approx 0.6 \text{ m}$). On the opposite, in in-file conditions, the modal distance decreases significantly from $\approx 1.3 \text{ m}$ in free-flow to $\approx 0.9 \text{ m}$ at $\rho \approx 1.3 \text{ p/m}^2$. These different trends showcase the importance of treating the abreast and in-file condition separately.

To quantitatively investigate how the formation changes with respect to the dyad and crowd state, we introduced a new scalar variable mapping the log-likelihoods of dyad formations: Π_{OLO} . Π_{OLO} provides a probabilistic measure of the relative preference (indeed, the observational likelihood) for abreast versus in-file formations in dependence on the crowd state. Conceptually, Π_{OLO} can also be interpreted as the difference in energy of the abreast and in-file state for a given crowding conditions - with dyads

willing to maximize their energy under a Boltzmann-like assumption. Through Π_{OLO} we accurately traced the boundary ($\Pi_{OLO} = 0$) between abreast and in-file states, as the surrounding crowd state changes. This is indeed the state in which the dyad positional uncertainty is highest.

The most interesting regimes for the formation and Π_{OLO} are the counter-flow cases including its limits: free-flow (the surrounding crowd has 0 density) and standing crowd (the surrounding crowd has 0 velocity). We observed that up to $\rho \approx 0.7 \text{ p/m}^2$, Π_{OLO} has a non-monotonic trend in dependence on the dyad velocity: Π_{OLO} is typically closest to 0 when the dyad move slowly, likely portraying directional uncertainty. In addition, there are two, density-dependent, critical velocity values on which Π_{OLO} is minimum and maximum. These are the velocities with, respectively, lowest and highest likelihood of abreast state. These velocities are also lower and higher than the average dyad velocity for the same density. We conjecture that these velocities separate regimes of directional uncertainty, which also reverberates on the formation, and running regimes, in which abreast is opted for as much as possible. These two critical velocity merge at around $\rho \approx 0.7 \text{ p/m}^2$ and Π_{OLO} becomes monotonically decreasing with the dyad velocity. Notably, transitioning from standing crowd to counter-flow has little influence on Π_{OLO} . A counter-flowing crowd marginally reduces the density level and velocity-levels at which a given Π_{OLO} value is observed. In other terms, a counter-flowing crowd acts on the formation in the same way as a standing crowd of slightly higher density and velocity, “compressing” the density dynamic range.

We proposed a compact and accurate phenomenological model for Π_{OLO} hinging on the aforementioned density-dependent critical velocity values - which we fit as linear velocity-density relations. Effectively, Π_{OLO} (indeed its derivative with respect to the dyad velocity) behaves as the product of two traditional fundamental diagrams. As such, it can be modeled with few parameters and, overall, a cubic polynomial. Finally, in co-flowing states, Π_{OLO} typically indicates an abreast state, with uncertainty growing with density. It is worth mentioning that we willingly excluded an analysis of “sideways” crossings between crowd and dyads - limiting to the better defined counter- and co-flow states and limits thereof. Such sideways crossing condition rich of sub- and corner cases, whose complexity is left to forthcoming studies.

In general, our analysis opens the possibility of detailed microscopic modeling of dyad dynamics across various flow regimes. Indeed, given the prevalence of dyads in pedestrian crowds, this is instrumental towards accurate and generalizable models of group dynamics and, by extension, crowd dynamics as a whole, and to fundamental studies of the behavior of the dyads. Note that scaling the dyad detection and analysis to $\mathcal{O}(10^6)$ trajectories was essential to achieve the statistical resolution necessary to quantify configuration transitions in a systematic way - something inaccessible to analyses hinged on smaller datasets. The Π_{OLO} framework provides a compact, yet expressive scalar measure of dyad configuration, enabling potential integration of empirically-grounded group dynamics into both microscopic crowd-simulation models and macroscopic active-matter theories.

Acknowledgments

The authors wish to acknowledge Tom Harmsen who contributed initial implementations of the analysis through his Bachelor final project at TU/Eindhoven. The authors acknowledge the financial support of EAISI, Eindhoven Artificial Intelligence Systems Institute, through a starting grant.

References

1. Still GK. *Applied Crowd Science*. Crc Press; 2021.
2. Feliciani C, Corbetta A, Haghani M, Nishinari K. Trends in crowd accidents based on an analysis of press reports. *Safety Science*. 2023;164:106174. doi:10.1016/j.ssci.2023.106174.
3. Corbetta A, Toschi F. Physics of Human Crowds. *Annual Review of Condensed Matter Physics*. 2023;14(1):311-33. doi:10.1146/annurev-conmatphys-031620-100450.
4. Adrian J, Amos M, Appert-Rolland C, Baratchi M, Bode N, Boltes M, et al. Glossary for Research on Human Crowd Dynamics - 2nd Edition. *Collective Dynamics*. 2025 05;10:1-32. doi:10.17815/CD.2025.189.
5. Moussaïd M, Perozo N, Garnier S, Helbing D, Theraulaz G. The Walking Behaviour of Pedestrian Social Groups and Its Impact on Crowd Dynamics. *PLOS ONE*. 2010;5(4):1-7. Publisher: Public Library of Science. doi:10.1371/journal.pone.0010047.
6. Feliciani C, Jia X, Murakami H, Ohtsuka K, Vizzari G, Nishinari K. Social groups in pedestrian crowds as physical and cognitive entities: Extent of modeling and motion prediction. *Transportation Research Part A: Policy and Practice*. 2023 10;176:103820. doi:10.1016/j.tra.2023.103820.
7. Hu Y, Zhang J, Song W, Bode NWF. Social groups barely change the speed-density relationship in unidirectional pedestrian flow, but affect operational behaviours. *Safety Science*. 2021;139:105259. doi:10.1016/j.ssci.2021.105259.
8. Ye R, Fang Z, Lian L, Wang Q, Zeng G, Cao S, et al. Traffic dynamics of uni- and bidirectional pedestrian flows including dyad social groups in a ring-shaped corridor. *Journal of Statistical Mechanics: Theory and Experiment*. 2021;2021(2):023406. doi:10.1088/1742-5468/abdc1a.
9. Zanlungo F, Kanda T. Do walking pedestrians stably interact inside a large group? Analysis of group and sub-group spatial structure. *Proceedings of the Annual Meeting of the Cognitive Science Society*. 2013;35(35). Available from: <https://escholarship.org/uc/item/03s4x9st>.
10. Nicolas A, Hassan FH. Social groups in pedestrian crowds: review of their influence on the dynamics and their modelling.

Transportmetrica A: Transport Science. 2023;19(1):1970651.
doi:10.1080/23249935.2021.1970651.

11. Seer S, Brändle N, Ratti C. Kinects and human kinetics: A new approach for studying pedestrian behavior. *Transportation Research Part C: emerging technologies*. 2014;48:212-28.
doi:10.1016/j.trc.2014.08.012.
12. Pouw CA, Corbetta A, Gabbana A, Van Der Laan C, Toschi F. High-statistics pedestrian dynamics on stairways and their probabilistic fundamental diagrams. *Transportation Research Part C: emerging technologies*. 2024;159:104468.
doi:10.1016/j.trc.2023.104468.
13. Gu F, Guiselin B, Bain N, Zuriguel I, Bartolo D. Emergence of collective oscillations in massive human crowds. *Nature*. 2025;638(8049):112-9. doi:10.1038/s41586-024-08514-6.
14. Parisi DR, Sartorio AG, Colonnello JR, Garcimartín A, Pugnaloni LA, Zuriguel I. Pedestrian dynamics at the running of the bulls evidence an inaccessible region in the fundamental diagram. *Proceedings of the National Academy of Sciences*. 2021;118(50):e2107827118. doi:10.1073/pnas.2107827118.
15. Corbetta A, Meeusen JA, Lee Cm, Benzi R, Toschi F. Physics-based modeling and data representation of pairwise interactions among pedestrians. *Physical Review E*. 2018;98(6):062310.
doi:10.1103/PhysRevE.98.062310.
16. Vleuten GGMvd, Toschi F, Schilders WHA, Corbetta A. Stochastic fluctuations of diluted pedestrian dynamics along curved paths. *Physical Review E*. 2024;109(1):014605.
doi:10.1103/PhysRevE.109.014605.
17. Gabbana A, Toschi F, Ross P, Haans A, Corbetta A. Fluctuations in pedestrian dynamics routing choices. *Proceedings of the National Academy of Sciences Nexus*. 2022;1(4):pgac169.
doi:10.1093/pnasnexus/pgac169.
18. Minartz K, Hendriks F, Koop SM, Corbetta A, Menkovski V. Discovering interaction mechanisms in crowds via deep generative surrogate experiments. *Scientific Reports*. 2025;15(1):10385.
doi:10.1038/s41598-025-92566-9.
19. Garcimartín A, Maza D, Pastor JM, Parisi DR, Martín-Gómez C, Zuriguel I. Redefining the role of obstacles in pedestrian evacuation. *New Journal of Physics*. 2018;20(12):123025.
doi:10.1088/1367-2630/aaf4ca.
20. Bonnemain T, Butano M, Bonnet T, Echeverría-Huarte I, Seguin A, Nicolas A, et al. Pedestrians in static crowds are not grains, but game players. *Physical Review E*. 2023;107(2):024612.
doi:10.1103/PhysRevE.107.024612.
21. Hu Y, Ren X, Zhang J, Song W. An experimental study on the movement characteristics of a social group in unidirectional flow. *Transportmetrica A: Transport Science*. 2023;19(1):2017066.
doi:10.1080/23249935.2021.2017066.

22. Crociani L, Gorrini A, Feliciani C, Vizzari G, Nishinari K, Bandini S. Micro and Macro Pedestrian Dynamics in Counterflow: The Impact of Social Group. In: Hamdar SH, editor. *Traffic and Granular Flow '17*. Springer International Publishing; 2019. p. 151-8. doi:10.1007/978-3-030-11440-4_18.
23. Gorrini A, Crociani L, Vizzari G, Bandini S. Crossing Behaviour of Social Groups: Insights from Observations at Non-signalised Intersection. In: Hamdar SH, editor. *Traffic and Granular Flow '17*. Springer International Publishing; 2019. p. 443-50. doi:10.1007/978-3-030-11440-4_48.
24. Gorrini A, Vizzari G, Bandini S. Granulometric Distribution and Crowds of Groups: Focusing on Dyads. In: Knoop VL, Daamen W, editors. *Traffic and Granular Flow '15*. Springer International Publishing; 2016. p. 273-80. doi:10.1007/978-3-319-33482-0_30.
25. Crociani L, Zeng Y, Vizzari G, Bandini S. Shape matters: Modelling, calibrating and validating pedestrian movement considering groups. *Simulation Modelling Practice and Theory*. 2018;87:73-91. doi:10.1016/j.smp.2018.06.001.
26. Zanlungo F, Yücel Z, Bršić D, Kanda T, Hagita N. Intrinsic group behaviour: Dependence of pedestrian dyad dynamics on principal social and personal features. *PLOS ONE*. 2017;12(11):e0187253. doi:10.1371/journal.pone.0187253.
27. Zanlungo F, Yücel Z, Kanda T. Intrinsic group behaviour II: On the dependence of triad spatial dynamics on social and personal features; and on the effect of social interaction on small group dynamics. *PLOS ONE*. 2019;14(12):e0225704. doi:10.1371/journal.pone.0225704.
28. Zanlungo F, Yücel Z, Kanda T. Social group behaviour of triads. Dependence on purpose and gender. *Collective Dynamics*. 2020;5:118-25. doi:10.17815/CD.2020.41.
29. Zanlungo F, Bršić D, Kanda T. Spatial-size scaling of pedestrian groups under growing density conditions. *Physical Review E*. 2015;91(6):062810. doi:10.1103/PhysRevE.91.062810.
30. Zanlungo F, Ikeda T, Kanda T. Potential for the dynamics of pedestrians in a socially interacting group. *Physical Review E*. 2014;89(1):012811. doi:10.1103/PhysRevE.89.012811.
31. Khan SD, Vizzari G, Bandini S, Basalamah S. Detection of Social Groups in Pedestrian Crowds Using Computer Vision. In: Battiatto S, Blanc-Talon J, Gallo G, Philips W, Popescu D, Scheunders P, editors. *Advanced Concepts for Intelligent Vision Systems*. Springer International Publishing; 2015. p. 249-60. doi:10.1007/978-3-319-25903-1_22.
32. Solera F, Calderara S, Cucchiara R. Socially Constrained Structural Learning for Groups Detection in Crowd. *IEEE Transactions on Pattern Analysis and Machine Intelligence*. 2016;38(5):995-1008. doi:10.1109/TPAMI.2015.2470658.

33. Li M, Chen T, Du H, Ma N, Xi X. Social group detection based on multi-level consistent behaviour characteristics. *Transportmetrica A: Transport Science*. 2023;19(1):1976877. doi:10.1080/23249935.2021.1976877.
34. Yücel Z, Zanlungo F, Ikeda T, Miyashita T, Hagita N. Deciphering the Crowd: Modeling and Identification of Pedestrian Group Motion. *Sensors*. 2013;13(1):875-97. doi:10.3390/s130100875.
35. Brščić D, Zanlungo F, Kanda T. Modelling of pedestrian groups and application to group recognition. In: 2017 40th International Convention on Information and Communication Technology, Electronics and Microelectronics (MIPRO); 2017. p. 564-9. doi:10.23919/MIPRO.2017.7973489.
36. Pouw CAS, Toschi F, Schadewijk Fv, Corbetta A. Monitoring physical distancing for crowd management: Real-time trajectory and group analysis. *PLOS ONE*. 2020;15(10):e0240963. doi:10.1371/journal.pone.0240963.
37. Liu W, Zhang J, Rasa AR, Li X, Ren X, Song W. Understanding step synchronization in social groups: A novel method to recognize group. *Physica A: Statistical Mechanics and its Applications*. 2023;628:129171. doi:10.1016/j.physa.2023.129171.
38. Gregorj A, Yücel Z, Zanlungo F, Kanda T. Gait synchronisation in pedestrian dyads: The influence of social interaction. *EPJ Web of Conferences*. 2025;334:04007. doi:10.1051/epjconf/202533404007.
39. Yücel Z, Zanlungo F, Shiomi M. Modeling the impact of interaction on pedestrian group motion. *Advanced Robotics*. 2018;32(3):137-47. doi:10.1080/01691864.2017.1421481.
40. Pouw CAS, van der Vleuten GG, Corbetta A, Toschi F. Data-driven physics-based modeling of pedestrian dynamics - dataset: Pedestrian trajectories at Eindhoven train station. Zenodo; 2024. doi:10.5281/zenodo.13784588.
41. Pouw CA, van der Vleuten GG, Corbetta A, Toschi F. Data-driven physics-based modeling of pedestrian dynamics. *Physical Review E*. 2024;110(6):064102. doi:10.1103/PhysRevE.110.064102.
42. Pouw C, Willems J, Schadewijk Fv, Thurau J, Toschi F, Corbetta A. Benchmarking high-fidelity pedestrian tracking systems for research, real-time monitoring and crowd control. *Collective Dynamics*. 2021;6:1-22. doi:10.17815/CD.2021.134.

Appendices

A Definition of the standing threshold v_s

To distinguish between standing and moving pedestrians, we analyze the speed distribution of pedestrians in our dataset (Fig 11). The distribution exhibits three distinct peaks: stationary pedestrians at $\approx 0.0 \text{ m/s}$, slow

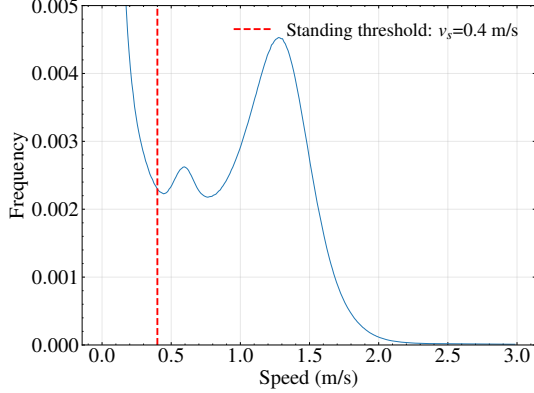


Fig 11. Probability density function of pedestrian speeds from twenty randomly selected days in our dataset. The red dashed line marks the standing threshold $v_s = 0.4$ m/s. Which is set between the stationary peak at 0.0 m/s and the slow-walking peak at 0.6 m/s.

walkers at ≈ 0.6 m/s, and normal walkers at ≈ 1.3 m/s. We set the standing threshold at $v_s = 0.4$ m/s, positioned between the stationary and slow-walking peaks.

B Modal distance definition

To extract characteristic interpersonal distances for each configuration type (abreast and in-file), we integrate the probability distributions $\mathbb{P}(x_r, y_r)$ over narrow bands around each principal axis (Fig 12a depicts the integration domains). In formulas, let

$$g^{\leftrightarrow}(x_r) = \int_{-\Delta b}^{\Delta b} \mathbb{P}(x_r, y_r) dy_r, \quad g^{\uparrow}(y_r) = \int_{-\Delta b}^{\Delta b} \mathbb{P}(x_r, y_r) dx_r \quad (51)$$

where $\Delta b = 0.15$ m defines the band width. As illustrated Fig 12b, we fit each marginal distribution with a Gaussian:

$$G(l) \propto \exp\left(-\frac{(l - \mu)^2}{2\sigma^2}\right), \quad (52)$$

where μ is the modal position and σ is the standard deviation. Finally, we define the interpersonal distance as twice the μ value, as in Eq 23 (cf. Fig 12b).

C Region of validity for the Π_{OLO} model

In Section 3.2 and 3.3.1, we provided phenomenological models for Π_{OLO} in standing crowd and counter-flow conditions, respectively. These models only defined in regions where sufficient data is available. Specifically, the model for $\Pi_{\text{OLO}}^{\text{standing}}(v_{\text{com}}, \rho)$ (Eq 44) has validity in the region

$$\{(v_{\text{com}}, \rho) : \rho_{\text{free}} = 0.16 \text{ p/m}^2 < \rho < A v_{\text{com}} + B, \quad v_{\text{com}} > v_s\}, \quad (53)$$

where $A = -1.2 \text{ ps/m}^3$, $B = 2.5 \text{ p/m}^2$. Whereas the model for $\Pi_{\text{OLO}}^{\text{counterflow}}(v_{\text{com}}, \rho)$ (Eq 50) has validity in

$$\{(v_{\text{com}}, \rho) : \rho_{\text{free}} < \rho < C v_{\text{com}}^2 + D v_{\text{com}} + E, \quad v_{\text{com}} > v_s\}, \quad (54)$$

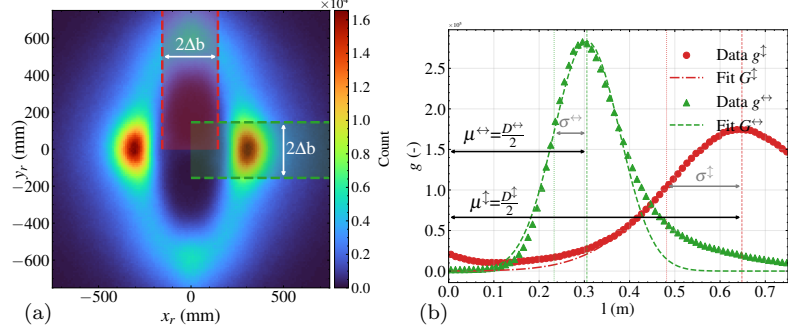


Fig 12. (a) Probability distribution $P(x_r, y_r)$, the bands in green and red indicate the integration domains for $g^{<>}(x_r)$ and $g^{>}(y_r)$ respectively (Eq 51). (b) The data points retrieved from the integrations for $g^{<>}$ in green triangles and $g^{>}$ in red circles with their corresponding G fits.

where $C = -0.35 \text{ ps}^2/\text{m}^4$, $D = 0.51 \text{ ps}/\text{m}^3$, and $E = 0.53 \text{ p}/\text{m}^2$. In Fig 13, we illustrate these valid regions.

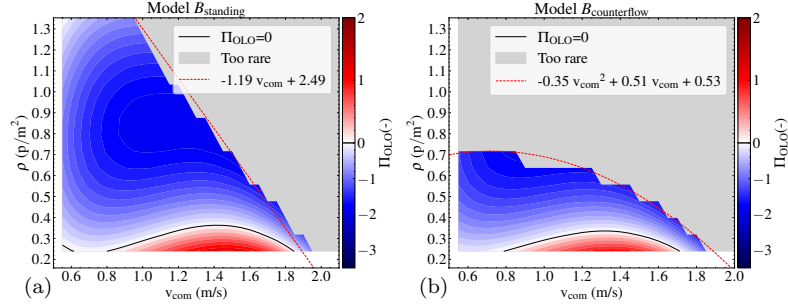


Fig 13. Models for $\Pi_{\text{OLO}}^{\text{standing}}(v_{\text{com}}, \rho)$ (Eq 44) and $\Pi_{\text{OLO}}^{\text{counterflow}}(v_{\text{com}}, \rho)$ (Eq 50), with their respective validity regions. (a) Standing crowd model (Eq 44) with validity boundary (dashed red line, Eq 53). (b) Counter-flow model (Eq 50) with validity boundary (dashed red line, Eq 54). Gray regions indicate insufficient data for reliable model predictions.